



Gremlin1 is a therapeutically targetable FGFR1 ligand that regulates lineage plasticity and castration resistance in prostate cancer

Chaping Cheng^{1,7}, Jinming Wang^{1,7}, Penghui Xu¹, Kai Zhang¹, Zhixiang Xin¹, Huifang Zhao¹, Zhongzhong Ji¹, Man Zhang², Deng Wang^{1,2}, Yuman He¹, Na Jing^{1,2}, Liancheng Fan¹, Kaiyuan Liu¹, Fei Li³, Chengcheng Liu¹, Yiming Gong¹, Suli Cui⁴, Zhe Sun⁴, Di Sun⁴, Xinlai Yao⁴, Hongjun Li⁴, Jian Zhang⁵, Pengcheng Zhang⁶, Baijun Dong⁶, Wei Xue¹, Xueming Qian⁴, Wei-Qiang Gao^{1,2}✉ and Helen He Zhu¹✉

Among the greatest hurdles in clinical management of prostate cancer (PCa) are the progression to lethal castration-resistant prostate cancer (CRPC) and the lack of suitable targeted therapies for advanced disease. Here we identify Gremlin1 as a ligand for fibroblast growth factor receptor 1 (FGFR1), which promotes lineage plasticity and drives castration resistance. Importantly, we generate a specific anti-Gremlin1 therapeutic antibody and demonstrate synergistic effect with androgen deprivation therapy (ADT) in CRPC. *GREM1* transcription is suppressed by androgen receptor (AR) and released following ADT. We show that Gremlin1 binds to FGFR1 and activates downstream MAPK signaling. Gremlin1 interacts with FGFR1 differently to its canonical ligand FGF1, as revealed through protein structure docking and mutagenesis experiments. Altogether, our data indicate Gremlin1 as a promising candidate therapeutic target for CRPC.

Androgen deprivation therapy is a mainstream treatment approach for PCa, which is one of the most common cancer types and leading causes of cancer-related death worldwide¹. ADT extends overall survival, but most patients who received this treatment progress to CRPC in a median time of 16–18 months^{2–4}. Second-generation antiandrogen drugs, such as enzalutamide, abiraterone and apalutamide, have been developed for CRPC by further inhibition of the AR pathway⁵. Potent second-generation ADT drugs usually achieve an excellent initial response but, unfortunately, disease recurrence still occurs rapidly and eventually leads to patient death⁶. Effective targeted therapy for CRPC is still lacking. Therefore, revealing novel treatment targets and developing new therapeutic strategies, including new antibody-based therapies, are major clinical objectives in regard to CRPC.

Gremlin1 is a highly conserved secreted protein in the differential screening-selected gene aberrative in the neuroblastoma (DAN) family of bone-morphogenetic protein (BMP) antagonists⁷. It was reported to bind to BMP2, BMP4 or BMP7 to form heterodimers and prevent interaction of BMP ligands with the corresponding BMP receptors, which subsequently inhibited the activation of BMP signaling⁷. Gremlin1 is a pivotal protein during embryogenesis^{8–10} and is closely related to tissue fibrotic lesions, as well as to glioma and colon cancer, by modulation of BMP signaling^{10–14}. However, our understanding of Gremlin1 as a secreted signaling protein is far from being in depth. In addition to the BMP signaling pathway,

whether Gremlin1 exerts its function through a non-BMP mechanism has not been elucidated.

Here, we report that Gremlin1 acts through a non-BMP-dependent mechanism and represents a new ligand of FGFR1 in advanced PCa; thus, it can serve as an important and promising therapeutic target for the treatment of CRPC, a deadly disease. Anti-Gremlin1 antibody exerts a strong tumor-inhibitory impact and displays a synergistic effect with ADT on CRPC.

Results

Gremlin1 positively correlates with tumor progression in PCa. Secreted proteins are a group of important potential therapeutic targets for anticancer drug development¹⁵. We analyzed the transcriptional levels of signaling-related secreted proteins on published PCa datasets¹⁶, and found that Gremlin1 was ranked one of the top differentially expressed proteins (Fig. 1a) in hormone-refractory PCa compared with hormone-naïve PCa. Gremlin1 expression levels were also found to be increased significantly in advanced metastatic CRPC compared with those in primary PCa, from the dataset of Yu et al.¹⁷ (Extended Data Fig. 1a). Analysis of the Beltran et al. 2016 CRPC cohort¹⁸ showed that Gremlin1 was most abundantly expressed in double-negative prostate cancer (DNPC), an emerging CRPC subtype in the post-second-generation antiandrogen era, that expresses neither neuroendocrine markers nor AR signaling molecules or low levels of AR signature genes^{19,20} (Extended Data Fig. 1b).

¹State Key Laboratory of Oncogenes and Related Genes, Renji-Med-X Stem Cell Research Center, Shanghai Cancer Institute & Department of Urology, Ren Ji Hospital, Shanghai Jiao Tong University School of Medicine, Shanghai, China. ²School of Biomedical Engineering & Med-X Research Institute, Shanghai Jiao Tong University, Shanghai, China. ³State Key Laboratory of Cell Biology, Shanghai Key Laboratory of Molecular Andrology, Shanghai Institute of Biochemistry and Cell Biology, CAS Center for Excellence in Molecular Cell Science, Chinese Academy of Sciences, Shanghai, China. ⁴Mabspace Biosciences (Suzhou) Co., Ltd, Suzhou, China. ⁵Key Laboratory of Cell Differentiation and Apoptosis of Chinese Ministry of Education & School of Pharmaceutical Sciences, Zhengzhou University, Zhengzhou, China. ⁶State Key Laboratory of Drug Research & Center of Pharmaceutics, Shanghai Institute of Materia Medica, Chinese Academy of Sciences, Shanghai, China. ⁷These authors contributed equally: Chaping Cheng, Jinming Wang. ✉e-mail: gao.weiqiang@sjtu.edu.cn; zhuhecrane@shsmu.edu.cn

Importantly, amplification of *GREMI* or a high *GREMI* messenger RNA level was associated with shortened disease/progression-free survival (TCGA, Firehose Legacy) (Extended Data Fig. 1c). Analysis of the SU2C 2019 PCa dataset²¹ also revealed that patients with elevated transcription of *GREMI* exhibited shorter overall survival (Extended Data Fig. 1d). We then performed Gremlin1 immunohistochemical (IHC) staining on a large cohort of 132 human PCa clinical samples collected at Ren Ji Hospital, School of Medicine, Shanghai Jiao Tong University. Among the 132 patient specimens, 55 were obtained from patients with CRPC. Quantitative study of IHC results showed a significantly enhanced staining intensity of Gremlin1 in CRPC samples compared with that in hormone-sensitive PCa (HSPC) (Fig. 1b,c). Patients with CRPC and higher Gremlin1 expression in tumor samples had a notably shorter overall survival and progression-free survival (Fig. 1d). Collectively, Gremlin1 is upregulated in CRPCs and strongly correlates with poor disease outcome.

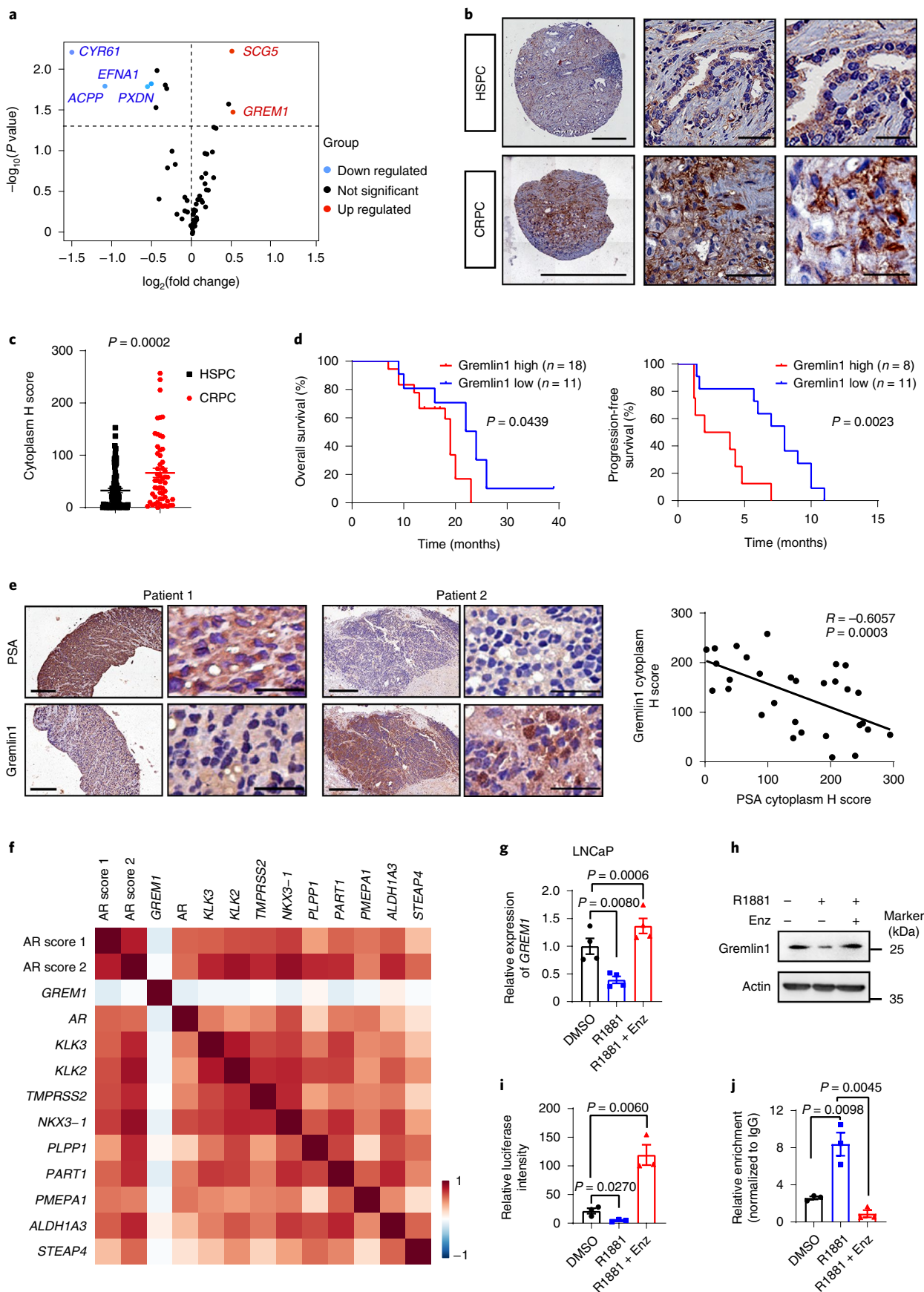
***GREMI* expression is repressed by AR and facilitated following ADT.** Androgen receptor plays a central role in PCa. To assess the relationship between Gremlin1 and AR signaling, we performed further IHC staining for Gremlin1 and prostate-specific antigen (PSA), a classic downstream target of AR, on sections of CRPC specimens. Statistical analysis showed that Gremlin1 expression was evidently upregulated in CRPCs with a low staining intensity of PSA (Fig. 1e). Furthermore, we found that *GREMI* mRNA levels displayed a strongly negative correlation with AR signature genes in the Beltran et al. CRPC cohort¹⁸ (Fig. 1f). We also observed a negative correlation between *GREMI* transcription expression and AR score in the SU2C 2019 PCa dataset²¹ (Extended Data Fig. 1e,f). There was a trend of shorter ADT treatment time in patients with high *GREMI* expression from the SU2C 2019 PCa cohort, although the difference between the *GREMI*^{low} and *GREMI*^{high} groups was not statistically significant ($P=0.0677$) (Extended Data Fig. 1g). We then asked whether the expression of Gremlin1 is regulated by AR signaling. Either an AR-expressing lentivirus or the CRISPR-Cas9 method was used to achieve AR upregulation in PCa cell lines LNCaP and LAPC4 (Extended Data Fig. 2a,c) or AR knockout in cell line LNCaP (Extended Data Fig. 2e). Immunoblotting and quantitative PCR (qPCR) experiments together showed that AR repressed the transcription of *GREMI* (Extended Data Fig. 2a–i). This conclusion is supported by experiments involving treatment with the AR agonist R1881 and antagonist enzalutamide (Fig. 1g,h). Moreover, a luciferase reporter assay showed that *GREMI* promoter-driven luciferase activity was greatly inhibited by treatment with R1881 but enhanced by the addition of enzalutamide (Fig. 1i). Chromatin immunoprecipitation (ChIP) experimental results further suggested the binding of AR to the promoter region of *GREMI* (Fig. 1j). These data support the concept that Gremlin1 is negatively regulated by AR.

To further understand the relationship between Gremlin1 and AR in CRPC cells, we utilized two pairs of hormone-naïve and CRPC cell lines—LNCaP versus LNCaP-R and VCaP versus VCaP-R. LNCaP-R was derived from xenografted LNCaP tumors implanted in castrated mice, while VCaP-R was generated by treatment of VCaP cells with charcoal/dextran-stripped serum for 3 weeks. As shown in Extended Data Fig. 2j,k, we observed higher mRNA expression of AR in LNCaP-R and VCaP-R cells than in their corresponding control cells. In prostate cells, androgen binds to AR to trigger a conformational change, resulting in AR nuclear translocation and subsequent transcriptional control of AR target genes. To address the regulation of androgen-bound AR on *GREMI* expression, we performed a dihydrotestosterone (DHT) induction experiment on LNCaP, VCaP, LNCaP-R and VCaP-R cells. As shown in Extended Data Fig. 2l,m, repression of AR on *GREMI* transcription required a high DHT concentration (10 nM), which stands in contrast to a much lower level of DHT (0.1 nM) required for transcriptional induction of the classic AR-activated gene *KLK3*. Furthermore, we used ChIP-qPCR to assess AR–chromatin binding following DHT treatment at different concentrations. Recruitment of AR to the *GREMI* gene required a higher concentration of DHT than that needed for the binding of AR to the *KLK3* gene. Together these results demonstrate that the transcriptional suppression of AR on *GREMI* depends on a high androgen concentration (Extended Data Fig. 2n,o).

Gremlin1 drives CRPC cell proliferation and tumor growth.

To explore the role of Gremlin1 in the progression of CRPC, we utilized AR-dependent PCa cell lines LNCaP and LAPC4, as well as AR-independent PCa cell line PC3. Cell sublines with loss or gain of Gremlin1 expression were generated (Fig. 2a and Extended Data Fig. 3a,h). *GREMI* knockdown in PCa cell lines suppressed sphere-forming capacity (Fig. 2b and Extended Data Fig. 3b) and cell growth (Fig. 2c and Extended Data Fig. 3c) and increased cell apoptosis (Extended Data Fig. 3d). *GREMI* overexpression, or the addition of Gremlin1 protein in culture medium, resulted in a significant elevation in sphere formation and cell proliferation compared with the corresponding control sublines (Fig. 2b,c and Extended Data Fig. 3b,c,i,j). Moreover, *GREMI* knockdown greatly potentiated the inhibitory effect of enzalutamide while *GREMI* overexpression or the addition of Gremlin1 protein led to a compromised response to enzalutamide treatment in LNCaP and LAPC4 cells (Fig. 2c–e and Extended Data Fig. 3j,k). Furthermore, exogenous expression of Gremlin1 in hormone-sensitive PCa organoids generated from the *Hi-Myc* mouse, a genetically engineered mouse model (GEMM) for PCa, promoted organoid growth under the ADT condition (Fig. 2f,g). We found that knockdown of *GREMI* markedly suppressed PC3 tumor growth and cell survival in vivo, while overexpression of *GREMI* enhanced tumor growth and tumor formation incidence in a limiting dilution assay (Extended Data Fig. 3e–g).

Fig. 1 | Gremlin1 is highly expressed in CRPC and is negatively regulated by AR. **a**, Differential expression of secreted signaling proteins in hormone-naïve PCa compared with hormone-refractory PCa (data obtained from Oncomine PCa dataset¹⁶). **b**, IHC staining images of Gremlin1 in HSPCs and CRPCs ($n=77$ HSPC samples, $n=55$ CRPC samples). Representative images are presented. Scale bars: left panels, 500 μm ; middle panels, 50 μm ; right panels, 20 μm . **c**, Gremlin1 staining intensity is significantly higher in CRPCs than in HSPCs ($n=77$ HSPC samples, $n=55$ CRPC samples). Cytoplasm H scores were analyzed with Aperio ScanScope software. **d**, Shorter overall survival and progression-free survival were found in patients with PCa and higher Gremlin1 expression ($P=0.0439$ and $P=0.0023$, respectively). **e**, IHC images of PSA and Gremlin1 in CRPCs. Scale bars: left panels in patient 1 and patient 2, 200 μm ; right panels in patient 1 and patient 2, 100 μm ; $n=30$, each dot represents tissue from an individual patient. **f**, Correlation analysis of *GREMI* mRNA level and AR signaling gene expression (data obtained from the Beltran et al. 2016 dataset¹⁸; $n=49$ tumor samples. AR score1 was adopted from the cBioPortal database containing 30 AR-responsive genes described previously⁴⁶. AR score 2 was calculated based on ten AR-responsive genes adopted from a previous publication¹⁹. **g–i**, *GREMI* mRNA transcription (**g**), Gremlin1 protein level (**h**) and *GREMI* promoter-driven luciferase activity (**i**) were downregulated following AR activation by R1881 (1 nM), and were significantly increased following AR inhibition by enzalutamide (Enz, 10 $\mu\text{g ml}^{-1}$) in LNCaP cells ($n=3$ independent samples). **j**, ChIP assay results showing enrichment levels of AR with Gremlin1 promoter in LNCaP cells following treatment with R1881 (1 nM) or enzalutamide (10 $\mu\text{g ml}^{-1}$) ($n=3$ independent samples). Two-tailed Student's *t*-test was used for statistical analyses, and log-rank (Mantel-Cox) test was used for survival analyses. Data presented as means \pm s.e.m.).



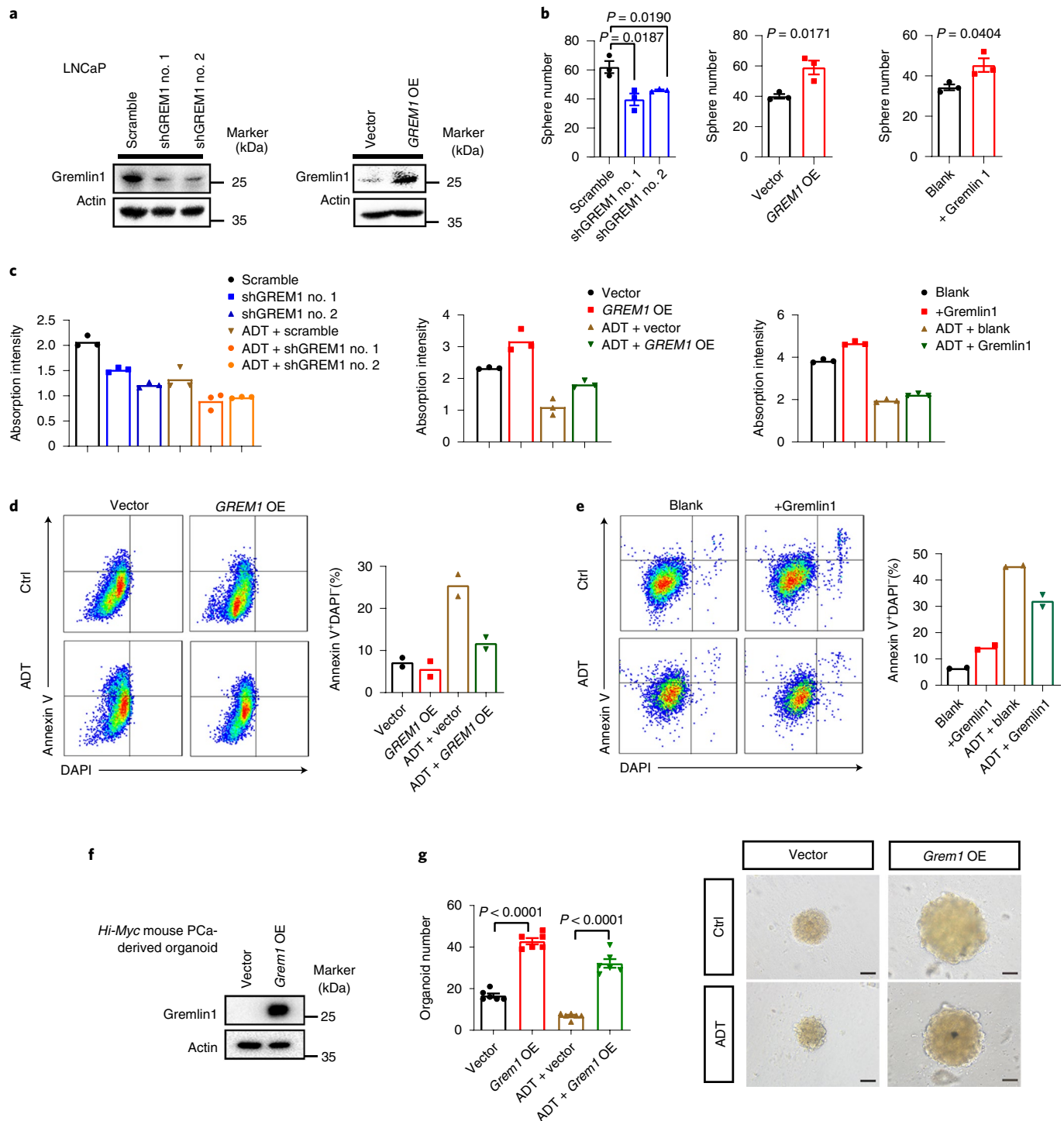


Fig. 2 | Gremlin1 facilitates the development of castration resistance in PCa cells. a, Immunoblotting confirmed the efficiency of *GREM1* knockdown and overexpression (OE) in LNCaP cells. Experiments were repeated at least three times, with similar results, and representative images are shown. **b**, *GREM1* knockdown inhibits sphere-forming ability in LNCaP cells, while overexpression of *GREM1* or external addition of Gremlin1 protein (100 ng ml^{-1}) exerts the opposite effect ($n = 3$ biological replicates). **c**, Gremlin1 promotes the growth of LNCaP PCa cells under ADT (treatment with enzalutamide at $10 \text{ } \mu\text{g ml}^{-1}$); $n = 3$ independent treated cell cultures. **d,e**, *GREM1* expression (**d**) and addition of exogenous Gremlin1 protein (**e**) repress cell apoptosis in LNCaP cells treated with ADT (treatment with enzalutamide at $10 \text{ } \mu\text{g ml}^{-1}$); $n = 2$ independent treated cell cultures; experiments were repeated at least three times. **f**, Overexpression of *GreM1* verified by immunoblotting in *Hi-Myc* mouse PCa-derived organoid. Experiments were repeated at least three times with similar results, and representative images are shown. **g**, Gremlin1 promotes organoid formation and ADT tolerance of *Hi-Myc* PCa organoids ($n = 6$ independent samples). ADT: treated with enzalutamide at $10 \text{ } \mu\text{g ml}^{-1}$. Scale bars, $100 \text{ } \mu\text{m}$. Two-tailed Student's *t*-test was used for statistical analyses. Data are presented as means \pm s.e.m. Ctrl, control. shGREM1, short hairpin RNA targeting *GREM1*.

Together, these data suggest a tumor-promoting role of Gremlin1 in PCa and the development of castration resistance.

Next, we investigated the potential impacts of Gremlin1 on AR signaling, cell lineage and stemness-related genes. As shown in Extended Data Fig. 4a,b, AR signaling was downregulated in *GREM1*-overexpressing LNCaP and LAPC4 cells compared with controls. Moreover, androgen response element (ARE)–luciferase reporter assays showed that AR-driven luciferase activity was inhibited upon *GREM1* overexpression (Extended Data Fig. 4c,d). We additionally found that *GREM1*-overexpressing LNCaP and LAPC4 cells expressed higher levels of stemness-related genes and basal cell lineage markers, and lower levels of luminal genes (Extended Data Fig. 4a,b). In contrast, we did not observe alterations in neuroendocrine gene expression upon *GREM1* overexpression. We further performed RNA-sequencing (RNA-seq) of *GREM1*-overexpressing LNCaP and *Hi-Myc* mouse organoid and their respective controls. Gene set enrichment analysis (GSEA) indicated consistent effects of *GREM1* overexpression on AR signaling and cell lineage signatures (Extended Data Fig. 4e,f). ChIP sequencing (ChIP-seq) results further indicated reduced AR–chromatin binding intensity at AR target genes in *GREM1*-overexpressing LNCaP cells (Extended Data Fig. 4g). These data suggest that Gremlin1 promotes the lineage plasticity of PCa cells from a luminal phenotype to a DNPC-like state with a basal/stem cell-feature transcriptional profile.

Oncogenic effect of Gremlin1 depends on FGFR1 activation. To address the mechanism involved, we carefully compared the transcriptional profiles of the *GREM1*-overexpressing LNCaP subline and its control cells. We listed the most significantly differentially expressed gene sets in Fig. 3a. FGFR and MAPK signaling were the top hits in upregulated signaling pathways. Further GSEA showed an enrichment in signaling by FGFR1 and activation of MAPK activity in LNCaP cells transfected with *GREM1*-expressing lentivirus (Fig. 3b).

To test whether Gremlin1 promotes FGFR–MAPK signaling, we first performed an analysis of the expression levels of the four FGFRs in samples from patients with CRPC in a published CRPC dataset¹⁸. As shown in Fig. 3c, because *FGFR1* was the most abundantly expressed FGFR in CRPC we subsequently examined FGFR1 activation following Gremlin1 treatment. We treated LNCaP-R and PC3 cells with Gremlin1 at different concentrations (1, 10 and 100 ng ml⁻¹) and examined the phosphorylation levels of FGFR1, MEK1/2 and ERK1/2. The known FGFR1 ligands FGF1 and FGF2 were used as positive controls. As shown in Fig. 3d and Extended Data Fig. 5a, Gremlin1 treatment led to an increase in p-FGFR1, p-MEK1/2 and p-ERK1/2 levels in a dose-dependent manner. We further found that activation of the FGFR1/MAPK axis by Gremlin1 was independent of BMP, because the addition of BMP4 did not alter the phosphorylation levels of FGFR1, MEK1/2 and ERK1/2 following Gremlin1 stimulation (Fig. 3e). Interestingly,

Gremlin1 induced a more prolonged activation of MAPK signaling than FGF1 and FGF2 (Fig. 3f,g). Activation of MAPK in response to Gremlin1 treatment was maintained at a high level for up to 1 h following the addition of Gremlin1, while MAPK signaling was most highly activated within 10 min following FGF1 or FGF2 stimulation and rapidly diminished afterwards (Fig. 3f,g). In addition, exogenous expression of Gremlin1 resulted in activation of the FGFR1/MAPK signaling axis in PC3 and LNCaP PCa cell lines (Extended Data Fig. 5b).

MAPK signaling can be activated through many membrane receptors besides FGFR. To test whether MAPK pathway activation by Gremlin1 occurs via FGFR, we constructed a *FGFR1* knock-out LNCaP-R subline by the CRISPR–Cas9 method. As shown in Fig. 3h, phosphorylation of ERK1/2 and MEK1/2 following treatment with Gremlin1 could be abrogated by *FGFR1* knockout. Additionally, Gremlin1-mediated promotion effects on PCa cell growth and sphere formation were abolished by knockout of *FGFR1* (Extended Data Fig. 5c–e). Activation of the FGFR1/MAPK signaling axis by Gremlin1 was attenuated by the FGFR1 inhibitor BGJ398 but not by the EGFR inhibitor erlotinib (Fig. 3i,j). Furthermore, as shown in Extended Data Fig. 5f,g, the PCa proliferation- and sphere-formation-promoting roles of Gremlin1 were significantly compromised by treatment with both BGJ398 and the MAPK inhibitor trametinib, but not by the addition of BMP4. These results indicate that the oncogenic effect of Gremlin1 is attributable to the activation of the FGFR1/MEK/ERK signaling pathway.

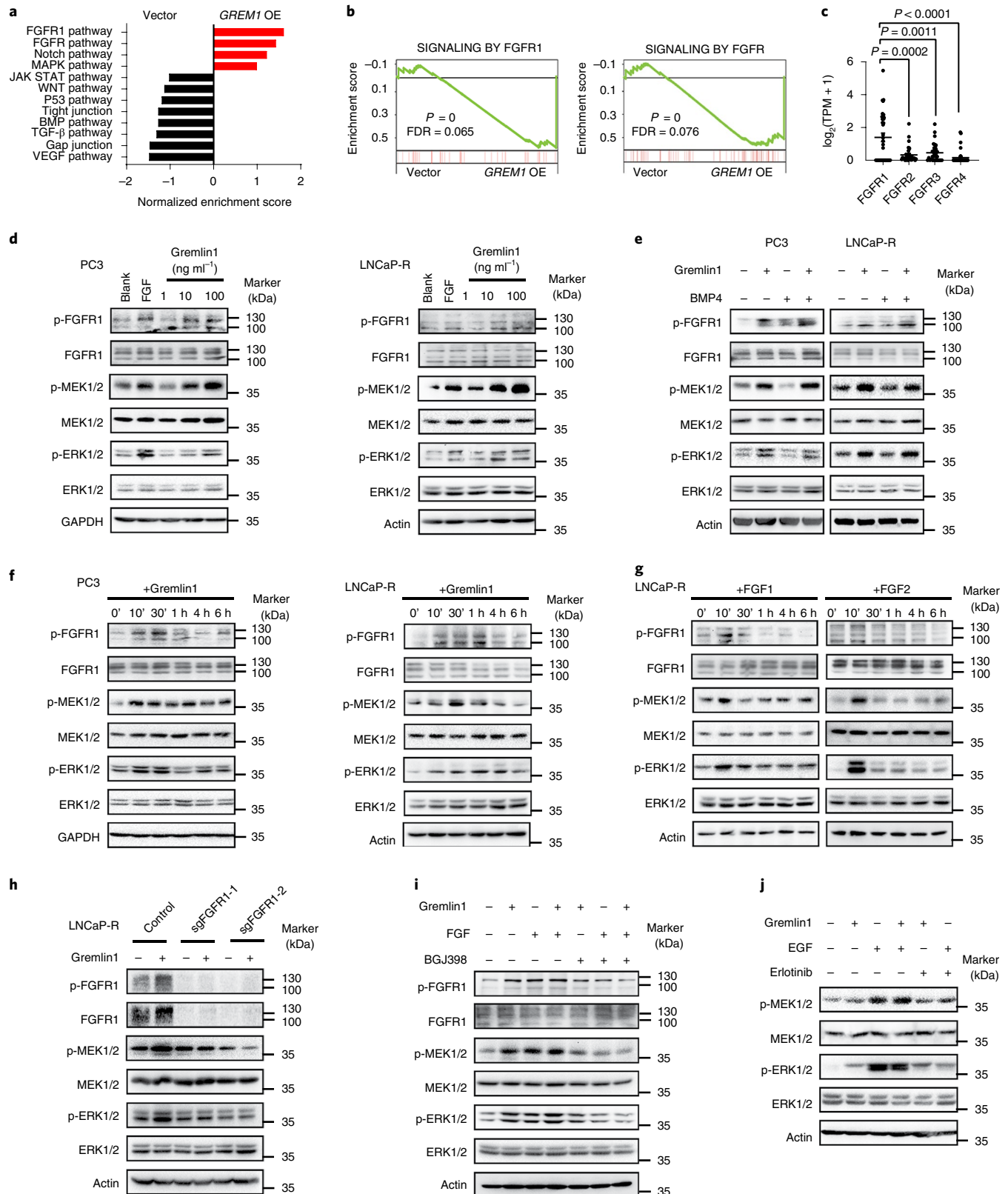
To explore whether Gremlin1/FGFR1 activation plays a role in castration resistance of PCa, we treated LNCaP cells transfected with vector or FGFR1 dominant active mutants²² (FGFR1-N546K and FGFR1-R656P) with ADT. Meanwhile, we knocked out *AR* in LNCaP cells and evaluated the effect of FGFR1 inhibition/activation or Gremlin1 addition on AR-independent PCa cell growth. As shown in Extended Data Fig. 5h,i, constitutive activation of FGFR1 signaling was sufficient to drive PCa cell proliferation under the ADT condition or upon *AR* knockout. Treatment with BGJ398 led to a severe reduction in LNCaP-sgAR cell growth, while the addition of Gremlin1 protein promoted AR-independent growth of LNCaP cells (Extended Data Fig. 5j). These data collectively imply a critical function of the Gremlin1/FGFR1 axis in the development of castration resistance in PCa.

Gremlin1 is a novel FGFR1 ligand in PCa. We next sought to identify the mechanism leading to activation of the FGFR1/MEK/ERK signaling pathway by Gremlin1 by performing surface plasmon resonance analysis (ForteBio). As shown in Fig. 4a, FGFR1 bound to Gremlin1 immobilized on a ForteBio sensor chip with high affinity ($K_D = 1.06 \times 10^{-8}$ M, K_D : Dissociation constant). ELISA assays demonstrated a specific interaction between FGFR1 and Gremlin1, because binding signals were not obtained between FGFR1 and Gremlin2 or BMP antagonists COCO and DAN

Fig. 3 | The oncogenic effect of Gremlin1 in PCa is dependent on activation of the FGFR1/MEK/ERK signaling pathway. **a**, Gene set enrichment analysis (GSEA) of RNA-seq data demonstrating that the FGFR1 and MAPK signaling pathways are the most enriched in the *GREM1*-overexpressed LNCaP subline. RNA-seq was performed on three independent samples. **b**, GSEA showing enrichments of the FGFR and FGFR1 signaling related genes in the *GREM1* overexpressed LNCaP subline. FDR: false discovery rate. **c**, *FGFR1* is the most abundantly transcribed FGFR in CRPC (data were obtained from the Beltran et al. 2016 dataset¹⁸; $n = 49$ tumor samples). TPM: Transcripts Per Kilobase Million. **d**, The FGFR1/MEK1/2/ERK1/2 signaling pathway is activated by Gremlin1 protein in PC3 cells and LNCaP-R cells in a dose-dependent manner. FGF1 (20 ng ml⁻¹) was used as a positive control to stimulate FGFR. **e**, Activation of the MEK/ERK signaling pathway by Gremlin1 is independent of BMP4. PC3 and LNCaP-R cells were treated with Gremlin1 protein (100 ng ml⁻¹) in the presence of BMP4 (20 ng ml⁻¹) or without BMP4. **f,g**, Treatment with Gremlin1 (100 ng ml⁻¹) (**f**) leads to more prolonged stimulation of FGFR1/MEK1/2/ERK1/2 signaling activation than FGF1 or FGF2 (20 ng ml⁻¹) (**g**). **h**, Activation of the FGFR1/MEK1/2/ERK1/2 signaling pathway is abrogated by CRISPR–Cas9-mediated *FGFR1* knockout. **i**, Gremlin1 activates the MEK/ERK signaling pathway through FGFR1. LNCaP-R cells were treated with Gremlin1 (100 ng ml⁻¹), FGF1 (20 ng ml⁻¹) or FGFR inhibitor BGJ398 (1 μM), as indicated. **j**, Activation of MEK/ERK signaling pathway by Gremlin1 is independent of EGFR. LNCaP-R cells were treated with Gremlin1 (100 ng ml⁻¹), EGF (20 ng ml⁻¹) or erlotinib (1 μM), as indicated. Immunoblotting experiments were repeated at least three times and representative images are shown. Two-tailed Student's *t*-test was used for statistical analyses. Data are presented as means ± s.e.m.

(Fig. 4b). Coimmunoprecipitation assays using exogenously expressed Flag-tagged Gremlin1 and HA-tagged FGFR1 in LNCaP cells (Fig. 4c) or endogenous proteins in LNCaP cells (Fig. 4d), and pulldown experiments using purified Gremlin1 and FGFR1 (extracellular region) proteins (Fig. 4e) together demonstrated a

direct physical association between FGFR1 and Gremlin1. We did not observe binding between Gremlin1 and other receptor tyrosine kinases such as EGFR (Fig. 4e). Furthermore, we conducted a bimolecular fluorescence complementation (BiFC) assay (Fig. 4f). *GREM1* and *FGFR1* complementary DNA, fused with fragments of



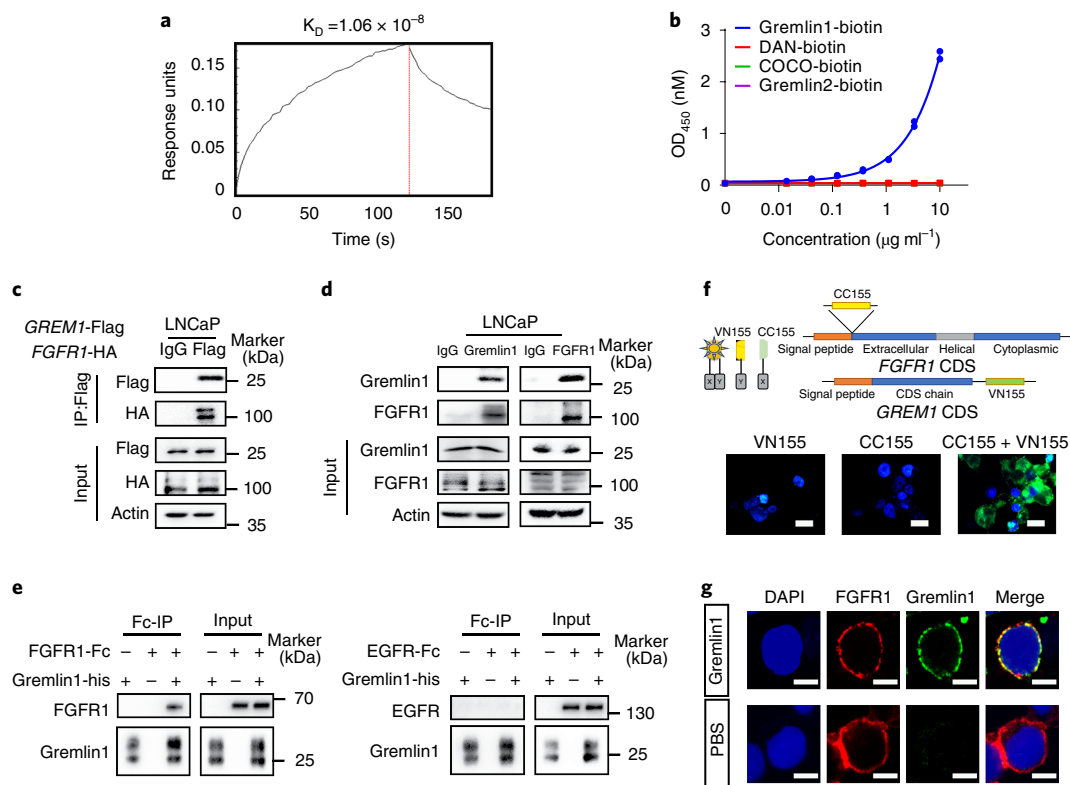


Fig. 4 | Gremlin1 is a novel FGFR1 ligand in CRPC. **a**, FGFR1 binds to Gremlin1-biotin immobilized on streptavidin sensor (ForteBio) ($K_D = 1.06 \times 10^{-8}$). Experiments were repeated at least twice, with similar results. **b**, ELISA showing that Gremlin1, but not Gremlin2 or other members of the DAN protein family, binds to FGFR1. Data presented as means \pm s.e.m.; $n = 2$ technical replicates; experiments were repeated twice. **c**, Gremlin1 coimmunoprecipitates with FGFR1 in LNCaP-R cells transfected with Flag-tagged Gremlin1- and HA-tagged FGFR1-expressing plasmids. Experiments were repeated at least three times with similar results, and representative images are shown. **d**, Endogenous Gremlin1 coimmunoprecipitates with FGFR1 in LNCaP-R cells. **e**, Interaction of purified Gremlin1 (400 mg ml^{-1}) and soluble FGFR1 protein (400 mg ml^{-1}) demonstrated by pull-down experiments. Experiments were repeated at least three times, with similar results. **f**, BiFC assay showing colocalization between Gremlin1 and FGFR1 in 293T cells. Scale bars, $20 \mu\text{m}$. BiFC assay with 293T cells was performed at least twice. Multiple fields of cell culture slides were examined during each repeat, and representative images are shown. CDS, coding sequence. **g**, Immunofluorescent staining images of Gremlin1 and FGFR1 in LNCaP-R cells. Cells were treated with Gremlin1 (100 ng ml^{-1}) or PBS for 10 min at 37°C . Scale bars, $10 \mu\text{m}$. The immunostaining experiment was repeated at least twice, with similar results. Multiple fields of cell culture slides were examined during each repeat, and representative images are shown. OD, optical density.

the coding sequence of yellow fluorescent protein (YFP), were transfected into 293 T cells individually or simultaneously. As shown in Fig. 4f, YFP signal could be detected only when *GREMI* and *FGFR1* plasmids were cotransfected. Consistent with this finding, confocal microscopic imaging of immunofluorescent staining showed colocalization of Gremlin1 and FGFR1 on the membrane of LNCaP-R cells (Fig. 4g). In addition, soluble FGFR1 could compete the binding between Gremlin1 and FGFR1, as revealed by a competitive ELISA experiment (Extended Data Fig. 6a). Consistently, activation of the FGFR1/MEK/ERK signaling pathway due to Gremlin1 could be attenuated by application of excessive amounts of soluble FGFR1 (Extended Data Fig. 6b). These data provide strong supporting evidence for specific binding between Gremlin1 and FGFR1, and support the notion that this binding is required for activation of FGFR1 and its downstream MAPK signaling (Extended Data Fig. 6b).

To further delineate the mode of Gremlin1–FGFR1 interaction, we performed coimmunoprecipitation between truncated FGFR1 (Fig. 5a,b) and Gremlin1 or the classic FGFR1 ligand FGF1. The extracellular region of FGFR1 consists of domain 1 (D1), domain 2 (D2) and domain 3 (D3)²³. Consistent with previous reports that the linker between D2 and D3 is the key binding area between FGF1 and FGFR1 (ref. ²³), we found that the loss of either D2 or D3 abolished coimmunoprecipitation of FGF1 and FGFR1. In contrast, only the loss of D2 abrogated the association between Gremlin1

and FGFR1, suggesting that Gremlin1 binds to FGFR1 at D2 (Fig. 5a,b). Moreover, we mutated the previously identified key amino acid residues of FGFR1 (C176 and R248) in its binding pocket to FGF1 (Extended Data Fig. 6c)^{24–26}. As expected, FGFR1-C176G or FGFR1-R248Q indeed disrupted coimmunoprecipitation of FGF1 and FGFR1 whereas these two mutations did not affect the interaction between Gremlin1 and FGFR1 (Extended Data Fig. 6c,d). These data indicated that FGFR1 binds to Gremlin1 in a way distinct from the binding mode with its classic ligand FGF1. In agreement with that, ForteBio assays, coimmunofluorescent staining and coimmunoprecipitation experiments together demonstrated that the addition of Gremlin1 did not compete for the association of FGF1 and FGFR1, and vice versa (Extended Data Fig. 6e–g). Additionally, we treated LNCaP cells with Gremlin1 in the presence of FGF1 at different concentrations and vice versa. As shown in Extended Data Fig. 6h, we observed additive effects in the phosphorylation of FGFR1, MEK1/2 and ERK1/2 between Gremlin1 and FGF1. Therefore, Gremlin1 and FGF1 probably bind at different sites of FGFR1. We then assessed the expression levels of Gremlin1 and various FGFs and their correlation in CRPC patient samples from a published RNA-seq dataset¹⁸ (Extended Data Fig. 6i,j). We observed that the *GREMI* transcript was higher than that of *FGFs* (Extended Data Fig. 6i). In addition, we measured the concentrations of Gremlin1 and FGF1 in prostatic fluid

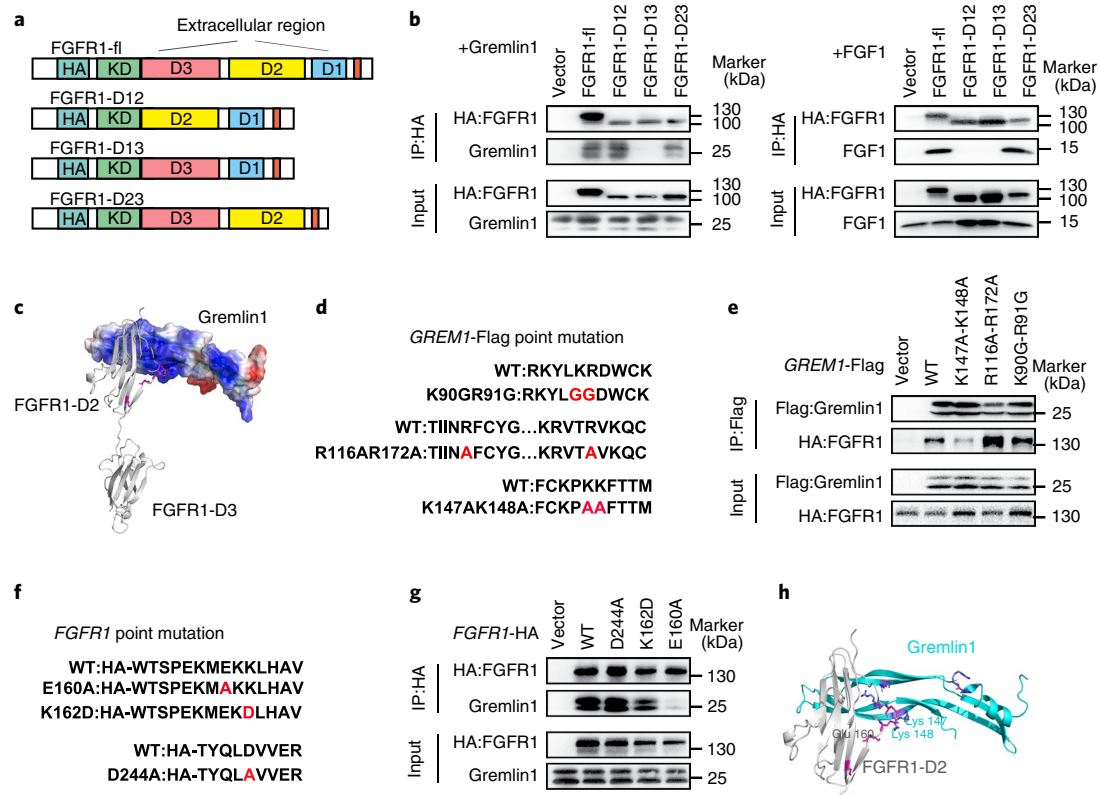


Fig. 5 | Lys147-Lys148 of Gremlin1 and Glu160 of FGFR1 are key amino acid residues in the binding pocket of the Gremlin1-FGFR1 protein complex.

a, Diagram of truncated FGFR1. **b**, Coimmunoprecipitation assay results comparing truncated FGFR1 with Gremlin1 (left) and with FGF1 (right). Experiments were repeated at least three times, with similar results. **c**, Predicted interaction of protein structures of Gremlin1 and FGFR1 extracellular domain initiated by HDOCK (<http://hdock.phys.hust.edu.cn/>). Protein structures were generated from PDB (<http://www.rcsb.org/>; Gremlin1: 5AEJ, FGFR1: 3OJV). **d**, Gremlin1 mutagenesis strategies (point mutations highlighted in red). **e**, Gremlin1 K147A-K148A mutant disrupts coimmunoprecipitation between Gremlin1 and FGFR1. Experiments were repeated at least three times, with similar results. **f**, Schematic of FGFR1 mutations (point mutations highlighted in red). **g**, Coimmunoprecipitation of FGFR1 and Gremlin1 is impaired by the FGFR1 E160A mutation. Experiments were repeated at least three times, with similar results. **h**, Docking module highlighting key amino acid residues in the binding pocket between Gremlin1 and FGFR1.

from patients with PCa using ELISA. As shown in Extended Data Fig. 6k, Gremlin1 (approximately 50 ng ml^{-1} on average) was more abundant than FGF1 (approximately 0.2 ng ml^{-1} on average) in prostatic fluid. These data collectively suggest that Gremlin1 serves as an important ligand for FGFR1 in CRPC.

Subsequently, we sought to decipher the structural basis of the Gremlin1-FGFR1 interaction. We used the HDOCK platform (<http://hdock.phys.hust.edu.cn/>) to perform docking of previously characterized protein structures of the Gremlin1 (PDB: 5AEJ)²⁷ and FGFR1 extracellular regions (PDB: 3OJV)²⁸. As shown in Fig. 5c, two positively charged clusters of amino acid residues in Gremlin1—denoted by blue in the docking model (Lys90-Arg91; R116-Lys147-Lys148-Arg172)—and extracellular D2 of FGFR1 were predicted to be an essential binding area between Gremlin1 and FGFR1. We then performed mutagenesis, as described in Fig. 5d,f, to test protein-binding simulation. Lys147-Lys148 to Ala147-Ala148 mutations in Gremlin1 or the corresponding E160A mutant of FGFR1 severely impaired coimmunoprecipitation between Gremlin1 and FGFR1 (Fig. 5e,g,h). Thus, Lys147-Lys148 of Gremlin1 and the corresponding Glu160 of FGFR1 are key amino acid residues in the formation of the Gremlin1-FGFR1 protein complex.

Gremlin1 antibody inhibits CRPC development in GEMM. The upregulation and oncogenic effect of Gremlin1 in CRPC make it a promising therapeutic target. To target Gremlin1, we developed a

monoclonal antibody against murine Gremlin1 with high affinity (Extended Data Fig. 7a). This antibody did not bind to Gremlin2 or other BMP antagonists such as COCO and DAN.

To determine the effect of anti-Gremlin1 antibody on PCa, we utilized an aggressive mouse model of CRPC, the *Pbsn-Cre4; Pten^{fl/fl}; Trp53^{fl/fl}* GEMM, which developed spontaneously invasive PCa at an average of 3 months^{29,30} (Fig. 6a). As shown in Fig. 6b, Gremlin1 was upregulated in *Pbsn-Cre4; Pten^{fl/fl}; Trp53^{fl/fl}* tumors compared with wild-type (WT) prostates, and was further enriched in castrated *Pbsn-Cre4; Pten^{fl/fl}; Trp53^{fl/fl}* tumors. Coimmunostaining of E-cadherin and Gremlin1 indicated that Gremlin1 is largely expressed by tumorous epithelial cells in castrated *Pbsn-Cre4; Pten^{fl/fl}; Trp53^{fl/fl}* tumors (Extended Data Fig. 7b). Notably, qPCR analysis of *Grem1* in several major organs of *Pbsn-Cre4; Pten^{fl/fl}; Trp53^{fl/fl}* mice demonstrated that its expression was highest in PCa tissue, which indicated that Gremlin1 is a plausible therapeutic target for PCa (Extended Data Fig. 7c).

We then evaluated the effect of anti-Gremlin1 antibody treatment on CRPC development in castrated *Pbsn-Cre4; Pten^{fl/fl}; Trp53^{fl/fl}* mice. Two-month-old *Pbsn-Cre4; Pten^{fl/fl}; Trp53^{fl/fl}* mice were castrated and subjected to anti-Gremlin1 antibody or control IgG treatment three times per week at 10 mg kg^{-1} for 8 weeks (Fig. 6a). Two months after castration, the animals were sacrificed for analysis. As shown in Fig. 6c,d, all control IgG-treated mice developed aggressive CRPC. Anti-Gremlin1 antibody exerted a profound repressive effect on PCa growth, as evidenced by marked

suppression of gross tumor size and weight and a significant reduction in proliferative PCNA-positive cells (Fig. 6e). Hematoxylin and eosin staining of prostate sections from anti-Gremlin1-treated *Pbsn-Cre4; Pten^{fl/fl}; Trp53^{fl/fl}* mice showed mostly intraductal hyperplasia with an intact basement membrane, which stands in marked contrast to the invasive PCa phenotype seen in IgG-injected mice (Fig. 6f). After treatment at 10 mg kg⁻¹ for 2 months, we observed no evident distinctions in major organs including the intestine, lung, liver, spleen, bone marrow and kidney, or alterations in peripheral blood cell count, between the two experimental groups (Extended Data Fig. 7d,e), suggesting minimal side effects.

To understand the underlying mechanism, we carried out RNA-seq on prostate samples from IgG- and Gremlin1 antibody-treated mice. Gene set enrichment analysis demonstrated that FGFR1 signaling was the most significantly changed signaling pathway in the Gremlin1 antibody-treated group (Fig. 6g,h). Further immunostaining and immunoblotting experiments confirmed that administration of Gremlin1 antibody resulted in considerable decrease in FGFR1, MEK1/2 and ERK1/2 phosphorylation (Fig. 6i,j). These results collectively show that reduced FGFR1/MAPK activation by Gremlin1 antibody contributes to its profound inhibitory impact on CRPC development in *Pbsn-Cre4; Pten^{fl/fl}; Trp53^{fl/fl}* mice. GSEA of RNA-seq data and qPCR experiments further suggested downregulation of stem cell-related and basal cell lineage genes, and upregulation of luminal lineage and AR signaling molecules, in the antibody-treated group (Extended Data Fig. 8), indicating reversal of lineage transition in PCa cells by the Gremlin1 antibody.

Gremlin1 antibody exerts antitumor effects in PCa cell lines. To target Gremlin1 in human PCa, we developed a monoclonal antibody against human Gremlin1. The affinity and specificity of this antibody to human Gremlin1 were verified by ELISA (Extended Data Fig. 9a). Anti-human Gremlin1 antibody exerted an inhibitory impact on proliferation and sphere formation in PC3 and LNCaP cells (Fig. 7a,b and Extended Data Fig. 9b,c). This antibody potentiated the antitumor effect of enzalutamide in AR-dependent LNCaP cells (Extended Data Fig. 9b,d). Biochemical analysis demonstrated dose-dependent inhibition of the FGFR1/MEK/ERK signaling pathway by anti-Gremlin1 antibody treatment in both PC3 and LNCaP cells (Fig. 7c and Extended Data Fig. 9e). To test the effect of anti-Gremlin1 antibody in CRPC in vivo, nude mice bearing the CRPC cell line PC3 xenografts were injected intraperitoneally (i.p.) with anti-Gremlin1 antibody or IgG three times per week for 2 weeks (10 mg kg⁻¹ body weight). Antibody against Gremlin1 blocked PC3 tumor growth (Fig. 7d,e). Meanwhile, FGFR1 knockout also significantly constrained PC3 growth in vivo. Gremlin1 antibody did not further repress xenografts of *FGFR1*-KO PC3 cells, suggesting that the effect of Gremlin1 is mediated via FGFR1 in vivo (Fig. 7d,e). On the other hand, knockout of *BMPR2*, the gene encoding bone morphogenetic protein receptor type-2, via CRISPR-Cas9 did not abrogate the inhibitory effect of anti-Gremlin1 antibody on PCa cells,

thus indicating a BMP signaling-independent role of anti-Gremlin1 antibody (Extended Data Fig. 9f,g). These data collectively demonstrate that a Gremlin1-specific antibody exerted a strong anti-tumor effect in CRPC, both in vitro and in vivo, by inhibition of FGFR1 signaling.

Synergistic effects of Gremlin1 antibody and ADT in CRPC.

We then tested the effect of anti-human Gremlin1 antibody on patient-derived organoids (PDOs) and xenografts (PDXs). Four previously established CRPC PDO lines³¹ from the Memorial Sloan Kettering Cancer Center were treated with anti-Gremlin1 antibody, enzalutamide or a combination of the two. We found that anti-human Gremlin1 antibody displayed a repressive role in PDO growth in two out of four PDO lines (Fig. 7f,g), an inhibitory effect that became more evident in serial PDO passage (Fig. 7f,g and Extended Data Fig. 9h). Enzalutamide treatment alone did not exert any effect on these four PDOs but showed an inhibitory impact on PDO growth in combination with anti-human Gremlin1 antibody (Fig. 7f,g). In addition, we assessed the endogenous levels of FGFR1 in these four organoids, BM1, BM61 and ST60, which were more sensitive to Gremlin1 antibody treatment and showed relatively higher FGFR1 expression compared with ST88 (Extended Data Fig. 9i). Furthermore, we tested the effect of FGFR1 inhibition in human organoids using BGJ398 and, as shown in Extended Data Fig. 9j, growth of human PCa organoids was suppressed. We did not find an additive effect between BGJ398 and Gremlin1 antibody (Extended Data Fig. 9j). We then tested the effects of anti-human Gremlin1 antibody in PDX in vivo. As shown in Fig. 7h,i, human CRPC PDX lines BM1 (ref.³¹) and MDA PCa 118b³² were resistant to ADT while Gremlin1-specific antibody exhibited tumor-inhibitory functions and displayed synergistic effects when applied in combination with enzalutamide. These data together demonstrate that antibody targeting Gremlin1 can serve as a promising therapeutic approach in patients with CRPC (Fig. 7j).

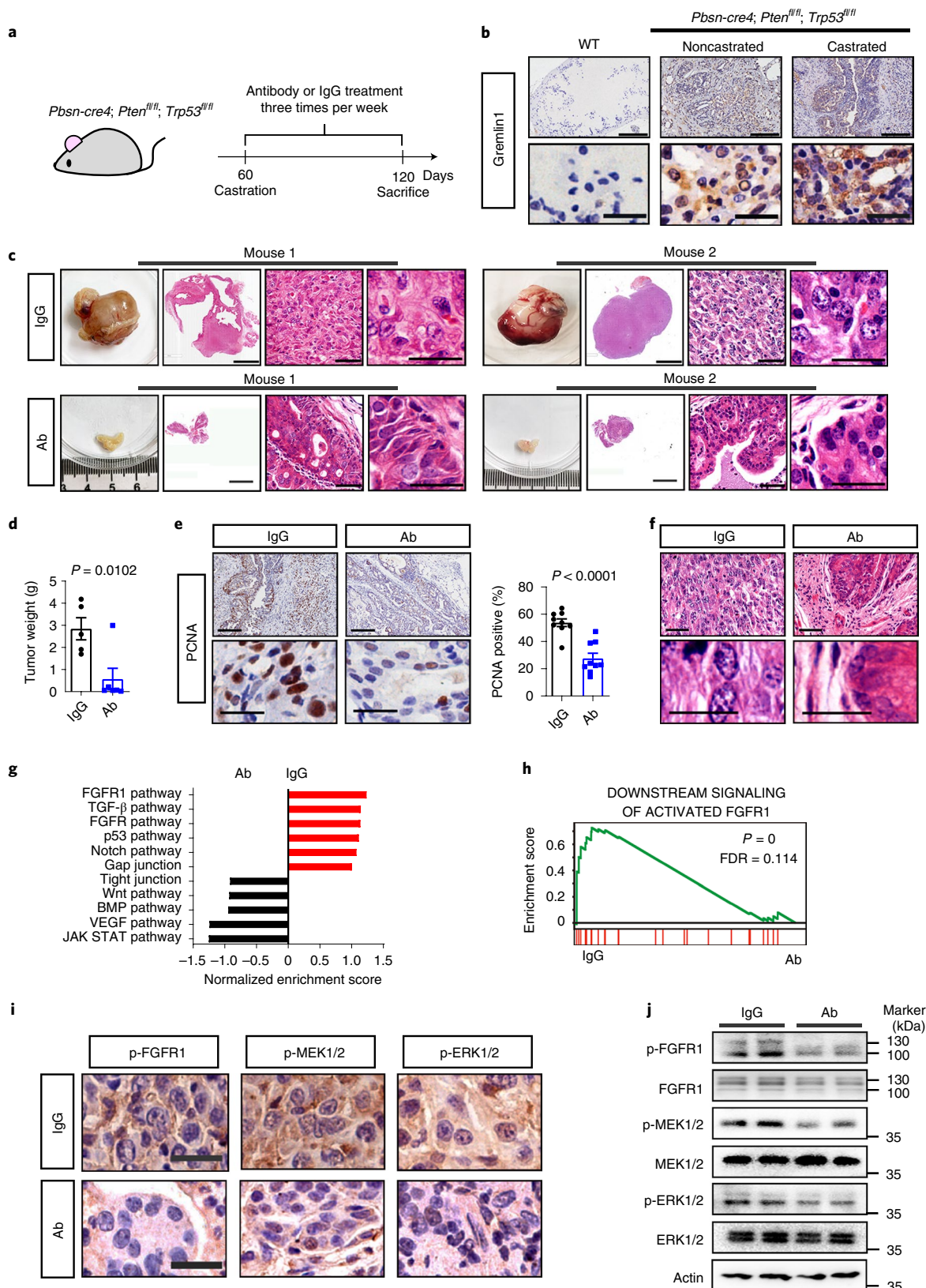
Discussion

Our study demonstrates an unexpected new function of Gremlin1 that is distinct from its previously well-known role as an antagonist of BMP⁷. We find that Gremlin1 promotes PCa progression and resistance to androgen deprivation through direct Gremlin1-FGFR1 binding to activate the FGFR1/MAPK signaling pathway. Neither activation of FGFR1/MAPK nor the tumor-promoting effects on PCa induced by Gremlin1 is affected by the addition of BMP4. Moreover, the anticancer effects of Gremlin1-blocking antibody on PCa cannot be overridden by *BMPR2* knockout, but are achieved by suppression of FGFR1 signaling. These results together support the premise that the Gremlin1/FGFR1/MAPK signaling axis drives PCa progression and points to Gremlin1 as an important therapeutic target in advanced PCa. Using coimmunostaining, BiFC, ForteBio, coimmunoprecipitation, pulldown and computer simulation approaches, we provide compelling evidence that Gremlin1 can directly bind to FGFR1. Of note, the binding

Fig. 6 | Gremlin1 antibody profoundly inhibits CRPC development in a *Pbsn-Cre4; Pten^{fl/fl}; Trp53^{fl/fl}* GEMM. **a**, Schematic illustrating treatments administered to a *Pbsn-Cre4; Pten^{fl/fl}; Trp53^{fl/fl}* GEMM. Mice that were castrated at 2 months received anti-Gremlin1 antibody (Ab) (10 mg kg⁻¹ i.p.) or IgG, as indicated, three times per week for 2 months. **b**, Gremlin1 highly expressed in the castrated *Pbsn-Cre4; Pten^{fl/fl}; Trp53^{fl/fl}* murine PCa model. Representative images of Gremlin1 immunostaining are presented. Scale bars: top, 200 μm; bottom, 25 μm. The experiment was performed on three mice per group. **c–e**, Anti-Gremlin1 antibody (10 μg ml⁻¹) exerts a significant inhibitory effect on PCa growth. Obvious suppression is evidenced by gross tumor appearance (**c**; scale bars: left, 1 cm; middle, 5 mm; right, 50 μm), tumor weight (**d**; IgG: *n* = 5 tumors; Ab: *n* = 6 tumors) and a significant reduction in PCNA-positive cells (**e**; *n* = 9 samples; scale bars: top, 200 μm; bottom, 25 μm). **f**, Anti-Gremlin1 treatment markedly represses the development of invasive PCa in castrated *Pbsn-Cre4; Pten^{fl/fl}; Trp53^{fl/fl}* mice. Scale bars, 50 μm. Experiments were performed with at least three independent tumor sections. **g**, GSEA indicates significant suppression of the FGFR1 signaling pathway in prostates of anti-Gremlin1 treatment group. **h**, GSEA showing downregulation of the FGFR1 signaling pathway in the group of anti-Gremlin1 treatment. FDR, false discovery rate. **i, j**, Immunostaining (**i**) and immunoblot analysis (**j**) showing inhibitory effects of anti-Gremlin1 antibody on the FGFR1/MAPK signaling pathway in prostates of *Pbsn-Cre4; Pten^{fl/fl}; Trp53^{fl/fl}* mice. The experiment was performed on three mice per group. Scale bars, 25 μm; two-tailed Student's *t*-test was used for statistical analyses. Data are presented as means ± s.e.m.

between Gremlin1 and FGFR1 is different from that in the FGFR1–FGFR1 interaction. While previous reports have shown that the linker between D2 and D3 in FGFR1 is an essential binding pocket of FGFR1 to FGF1 (ref. 23), in the current study we discovered that

Gremlin1 binds to D2 of the FGFR1 extracellular region and that Glu160 of FGFR1 and Lys147–Lys148 of Gremlin1 are key residues for Gremlin1/FGFR1 binding, based on protein structure docking and further mutation experiments. These results, together, strongly



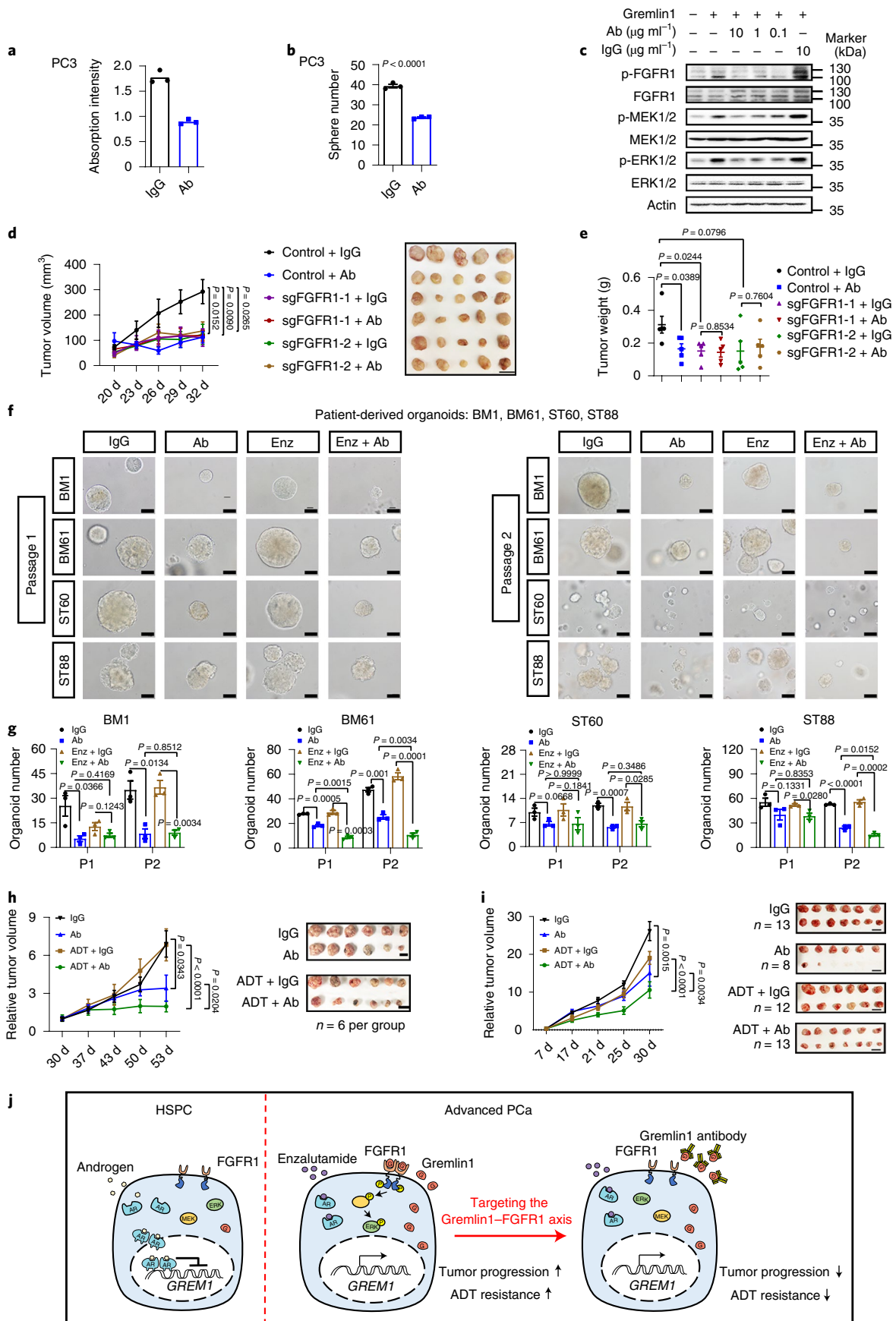


Fig. 7 | Synergistic effect of Gremlin1 antibody and enzalutamide in growth suppression of organoids and PDXs derived from patients with CRPC. **a**, The antibody against human Gremlin1 ($10 \mu\text{g ml}^{-1}$) represses cell proliferation of PC3 cells ($n = 3$ independently treated cell cultures). **b**, Anti-Gremlin1 antibody ($10 \mu\text{g ml}^{-1}$) exerts an inhibitory effect on sphere formation in PC3 cells ($n = 3$ biological replicates). **c**, Gremlin1 antibody neutralizes the activation of FGFR1/MEK1/2/ERK1/2 signaling induced by Gremlin1 protein (100 ng ml^{-1}) in PC3 cells in a dose-dependent manner. Experiments were repeated at least three times, with similar results. **d,e**, Gremlin1 antibody treatment or FGFR1 knockout significantly suppresses growth of PC3 cells in nude mice, as measured by tumor volume (**d**) and weight (**e**). Gremlin1 antibody was administered i.p. three times per week at 10 mg kg^{-1} . $n = 5$ mice; scale bars, 1 cm. **f**, Anti-Gremlin1 antibody ($10 \mu\text{g ml}^{-1}$) demonstrates strong inhibitory impact on organoids derived from patients with PCa, and shows a synergistic antitumor effect with enzalutamide as demonstrated in serial organoid-forming assays. Four previously reported PDO lines (BM1, BM61, ST60 and ST88) were tested in these experiments³¹. Scale bars, $50 \mu\text{m}$. **g**, Quantification of PDO numbers under IgG, Gremlin1 antibody, ADT and ADT+Gremlin1 antibody treatments during serial passages ($n = 3$ biological replicates). **h,i**, Anti-Gremlin1 antibody ($10 \mu\text{g ml}^{-1}$) slows in vivo growth of two PDX lines derived from patients with PCa and exerts synergistic inhibition on tumor growth with enzalutamide (10 mg kg^{-1}) in PDX line BM1 (ref. ³¹) (left) and PDX line MDA PCa 118b³² (right). Treatment was started when tumors reached around 200 mm^3 . Relative tumor volume at 30–53 days (**h**) and 7–30 days (**i**). Antibody was given three times per week (10 mg kg^{-1} i.p.). Final tumor size was standardized individually to pretreatment tumor. ADT: enzalutamide was administered orally 5 days per week at 10 mg kg^{-1} after castration. Scale bars, 1 cm. $n = 12$ mice in the BM1 experiment; for MDA PCa 118b, $n = 13, 8, 12$ and 13 mice in groups IgG, Gremlin1 antibody, ADT + IgG and ADT + Gremlin1 antibody, respectively. **j**, Schematic showing that Gremlin1 is transcriptionally upregulated after ADT therapy in CRPC. Gremlin1 acts as a novel ligand for FGFR1 to drive the activation of downstream MAPK signaling for castration-resistant growth of PCa. Targeting Gremlin1 using monoclonal antibody can serve as an attractive therapeutic approach for the treatment of advanced PCa. Two-tailed Student's *t*-test was used for statistical analyses, and two-way ANOVA analysis for the measurement of tumor volume.

support the view that Gremlin1 is a new ligand for FGFR1. More broadly, the FGFR signaling pathway is also known as a pivotal oncogenic driver in other tumors such as bladder cancer³³, gastric cancer³⁴, lung cancer³⁵ and breast cancer³⁶. Further study is warranted to determine whether the Gremlin1/FGFR1/MAPK axis is involved in tumorigenesis and progression in other cancer types. Following the wide application of second-generation ADT drugs for PCa in the clinic, the number of cases of AR-independent CRPC has increased significantly¹⁹. Among these cases, DNPC is an emerging AR-independent CRPC subtype that has been under-researched in the past¹⁹. In this study, we find that the expression of Gremlin1 in CRPC, particularly in DNPC, is abnormally increased compared with hormone-naïve or newly diagnosed PCa cases. The Gremlin1/FGFR1 axis promotes the AR independence of PCa cells, which is particularly relevant in light of recent findings that FGF signal activation is an essential molecular signature of DNPC and required for the AR-independent growth of DNPC¹⁹. Interestingly, we find that Gremlin1 upregulation in PCa leads to suppression of luminal and AR signaling molecules and increases in basal and stem cell-related gene expression, but not to alterations in neuroendocrine markers. Different groups have reported that lineage transition or neuroendocrine transdifferentiation is involved in the loss of ADT sensitivity^{19,20,37–40}. Although our data suggest that lineage plasticity may contribute to Gremlin1-mediated castration resistance, the mechanism of Gremlin1-driven lineage plasticity awaits future exploration.

Although second-generation antiandrogen drugs have been shown to trigger the upregulation of key drivers of AR-independent CRPC^{41,42}, the mechanism by which these drivers are modulated by AR signaling remains incompletely understood. We find that *GREMI* is negatively correlated with the AR signaling pathway in samples from patients with CRPC. *GREMI* transcription markedly increases when AR is knocked out or inhibited by enzalutamide. Conversely, AR activation leads to a decrease in *GREMI* expression in PCa cells. ChIP and luciferase reporter assay data, together, support the premise that suppression is achieved through binding of AR to the *GREMI* promoter region. Interestingly this repression requires a high DHT concentration, which stands in marked contrast to a much lower level of DHT required for transcriptional induction of the classic AR-activated gene *KLK3*. Therefore, inhibition of *GREMI* by AR is lifted upon treatment with strong AR antagonists such as enzalutamide. In abiraterone-treated PCa or in CRPC with low intratumor androgen levels, AR repression of *GREMI* transcription is also compromised. These mechanisms may explain the upregulation of Gremlin1 in advanced PCa.

Secreted proteins are an important category of drug targets for anticancer drug development⁴⁵. In this study, we developed monoclonal antibodies against human or murine Gremlin1. Based on experiments in human PCa cell lines, PDO and PDX, as well as in vivo studies on the *Pbsn-Cre4*; *Pten*^{fl/fl}; *Trp53*^{fl/fl} murine PCa model, we demonstrate a prominent tumor-inhibitory effect of Gremlin1 antibody on CRPC. However, we must take into consideration that Gremlin1 is also expressed in other tissues^{13,43,44}. A recent study has shown that conventional knockout of *GREMI* in mice causes abnormal development of the intestinal tract and a disorder of the hematopoietic system⁴⁵. In our study we carefully examined the main organs, including the intestines, of mice after Gremlin1 antibody treatment. At a dose of 10 mg kg^{-1} by i.p. injection three times per week, we observed neither obvious toxic effects, significant damage to the main organs nor altered peripheral blood cell counts. The minimal presence of side effects is probably attributable to the fact that the selective upregulation of Gremlin1 in PCa occurs after ADT. These observations suggest that application of Gremlin1 antibody in adults with a suitable dosing window may avoid unwanted side effects. The current work provides new insights into understanding of the molecular mechanisms of castration resistance development, and underscores the great therapeutic potential of Gremlin1 antibody in the treatment of CRPC.

Methods

Mice. All mouse experiments were conducted following protocols approved by the Ren Ji Hospital Laboratory Animal Use and Care Committee. Athymic nu/nu male mice (6 weeks old) and SCID mice were purchased from Shanghai Slac laboratory animal company. *Pbsn-Cre4*; *Pten*^{fl/fl}; *Trp53*^{fl/fl} mice were obtained from the Jackson Laboratory. *Hi-Myc* mice were provided by the NCI mouse repository. To test the therapeutic effect of Gremlin1 antibody on a PCa GEMM, *Pbsn-Cre4*; *Pten*^{fl/fl}; *Trp53*^{fl/fl} mice were castrated at the age of 2 months. Anti-murine Gremlin1 antibody or IgG was administered to castrated mice i.p. three times per week at 10 mg kg^{-1} for 8 weeks. All mice were sacrificed at approximately 2 months after castration and before tumor volume reached $2,000 \text{ mm}^3$. Prostate and other major organs were then harvested carefully, photographed and processed for further experiments. Peripheral blood was collected for complete blood cell count using a Sysmex pochH-100iVD machine (Sysmex).

Patient samples. The procedures of patient sample collection and analysis were approved by the Ethics Committee at Ren Ji Hospital, School of Medicine, Shanghai Jiao Tong University. Patients diagnosed with PCa and aged 50–85 years were recruited. Diagnosis of HSPC or CRPC was based on both histological examination and the expression of AR-related markers, by certified pathologists in the Department of Pathology, Ren Ji Hospital. A 149-spot, paraffin-embedded tissue microarray chip containing 67 paired prostate primary tumors and adjacent normal tissues, ten tumor tissues and five normal tissues, along with 55 paraffin-embedded PCa sections from patients with CRPC, was collected for IHC staining from the Urology Department of Ren Ji Hospital. Prostatic fluid was collected from patients

diagnosed with PCa at the Urology Department of Ren Ji Hospital. All specimens were obtained with patient informed consent.

Cell lines. Cell lines PC3, LNCaP and VCaP were obtained from the American Type Culture Collection. The LAPC4 cell line was kindly shared by C. Sawyers (Memorial Sloan Kettering Cancer Center). These cell lines were validated at Shanghai Biowing Applied Biotechnology by short tandem repeat profiling. LNCaP-R was derived from LNCaP cells implanted in castrated male nude mice. VCaP-R was generated from VCaP cells treated with charcoal/dextran-stripped serum (CSS3) (Gibco) for 3 weeks. PC3 and VCaP cells were grown in DMEM (Gibco), while LNCaP and LAPC4 were cultured in RPMI-1640 (Gibco). Both culture media were supplemented with 10% fetal bovine serum (FBS, Gibco) and 100 U ml⁻¹ penicillin/streptomycin (Gibco). LNCaP-R and VCaP-R cells were cultured in medium supplemented with 8% CSS3, 2% FBS and 100 U ml⁻¹ penicillin/streptomycin. Patient-derived organoid lines BM1, BM61, ST88 and ST60 were cultured and passaged according to the protocol published in ref. ³¹.

Plasmids. *GREM1* CDS (NM_013372.7) with a Flag tag or *FGFR1* CDS (a gift from J. Han) with a HA tag was cloned into a pLenti-CMV vector (GENOMEDITECH, no. GM-6172P1). The AR-expressing plasmid pLenti6.3/AR-GC-E2325 (Addgene, plasmid no. 85128, deposited by K.-H. Kalland) and plasmids containing fragments of YFP CDS (pBiFC-VN155152L, Addgene, no. 27097 and pBiFC-CC155, Addgene, no. 22015), both deposited by C.-D. Hu, were purchased from Addgene. For the BiFC experiment, VN155 was fused into the 3' end of the *GREM1* CDS sequence and CC155 was inserted into the *FGFR1* CDS between the signal peptide sequence and sequence encoding the extracellular domain. Short hairpin RNA was constructed to the GV248 vector (GENE.CHEM). Single guide RNA was designed using an online platform (www.benchling.com). The annealed DNA oligos were cloned into pLenti-CRISPRv2 (Addgene plasmid no. 52961, deposited by F. Zhang) for genome editing. Data from all shRNA and sgRNA sequencing used in this study are provided in Supplementary Table 1. *GREM1* promoter (chr15:32,716,990-32,720,976, hg38) and a luciferase CDS from the Firefly luciferase reporter vector pGL4.17(luc2/Neo) vector (Promega) were cloned into the pLenti-CMV vector for reporter assay.

Point mutations of Gremlin1 or FGFR1 were generated using site-directed mutagenesis by cloning entire *GREM1*- or *FGFR1*-expressing plasmids. Primers were created by CE Design (<https://crm.vazyme.com/cetool/en-us/singlepoint.html>). Truncated FGFR1 was cloned from a *FGFR1*-expressing plasmid by PCR. *BamHI* and *EcoRI* were used to perform pLenti-CMV vector linearization. All fragments and vectors were purified from agarose gel using the E.Z.N.A. Gel Extraction Kit (Omega, no. D2500-02) and assembled with the In-Fusion Cloning kit (Vazyme, no. C115) according to the manufacturers' protocols. Details of all primers used here are provided in Supplementary Table 1. All plasmids were verified by Sanger sequencing.

RNA-seq, ChIP-seq and sequencing data analyses. Total RNA was extracted from PC3, LNCaP cells or murine PCa samples using the Qiagen RNeasy kit according to the manufacturer's instructions (Qiagen). Libraries were generated using the NEBNext Ultra™ RNA Library Prep Kit for Illumina (NEB) and index codes were added to each sample. Adapters were cut by Cutadapt (v.2.6) and clean reads were then mapped to the human genome (GRCh38 release 84) using Hisat2 (v.2.1.0) with default settings. Gene expression quantification was calculated using Stringtie (v.1.3.6). Differential expression analysis was performed with DESeq2 (v.1.24.0). AR score 1 was acquired from the cBioPortal database (www.cbioportal.org), which contains 30 AR-responsive genes described previously⁴⁶. AR score 2 was calculated using the GSEA method (v.1.38.2) in R (v.3.6.1) based on ten AR-responsive genes adopted from a previous publication¹⁹. RNA-seq data on patients with PCa were accessed in dbGAP with accession phs000915.v2.p2 and analyzed using the same pipeline. GSEA was performed using GSEA (v.4.0.3) within MSigDBv7.1. CRPCs in the Beltran et al. cohort¹⁸ were divided into three subgroups (AR⁺CRPC (ARPC), AR⁻NE-PC (DNPC) and NEPC) using AR and NE scores generated by GSEA as previously described²⁰.

For ChIP-seq, immunoprecipitated DNA was used for ChIP-seq library preparation created by Novogene. Paired-end sequencing of samples was performed on the Illumina platform. Adapters were cut by Cutadapt (v.2.6) and clean reads were then mapped to the human genome (GRCh38 release 84) using bowtie2 (v.2.3.5) and SAMtools (v.1.9) with default settings. Picard (v.2.25.5) was used to remove duplicates. Heatmaps and summary plots were generated by deepTools (v.3.3.1).

Generation and validation of anti-Gremlin1 antibody. Anti-Gremlin1 antibodies were generated by immunization of mice with human Gremlin1 recombinant protein (ACRO Biosystems). Serum from immunized mice was analyzed for anti-Gremlin1 titer by ELISA assay. B cells isolated from the mouse with the highest anti-Gremlin1 titer were selected for further electrofusion with myeloma cells in log-phase growth status (SP2/0). Hybridoma cells were then collected, washed and plated into 96-well cell culture plates. Using the ELISA binding assay, clones with high binding affinity were selected. After two rounds of rescreening, lead antibodies were obtained and evaluated by ELISA assay and immunoblotting

to examine binding affinity, competitive binding ability and biological functions. The selected anti-mouse and anti-human Gremlin1 antibodies were then cloned and sequenced (Mabspace Biosciences). Plasmids containing anti-Gremlin1 antibody heavy- and light-chain genes were cotransfected into Expi-CHO cells (Gibco). After incubation at 37 °C under a humidified atmosphere of 5% CO₂ for 12–14 days, the cell suspension was harvested and centrifuged at 4,000g for 20 min. The cell culture supernatant was then filtered through a 0.22-μm filtration capsule to remove cell debris. The filtered supernatant was then loaded onto a pre-equilibrated Protein A affinity column. Protein A resin within the column was washed with equilibration buffer (PBS), and 25 mM citrate (pH 3.5) was used to elute the antibody. pH was adjusted to about 6.0–7.0 with 1 M Tris-base (pH 9.0). Endotoxin was kept below <1 EU mg⁻¹. Purified antibody was then characterized by SDS–polyacrylamide gel electrophoresis and size exclusion chromatography–high-performance liquid chromatography. The binding specificity of antibodies was carried out using ELISA with Gremlin1 and related proteins.

Anti-human Gremlin1 antibody (Mabspace Biosciences) was utilized to perform immunoblotting, immunofluorescence, IHC and immunoprecipitation assays. Specificity assessment of anti-human Gremlin1 antibody in all four assays was validated using *GREM1*-overexpressing and *GREM1* knockout LNCaP cells and their respective controls (Extended Data Fig. 10). The procedure for immunoprecipitation of LNCaP cell lysates was conducted as described below. Mass spectrometry of anti-human Gremlin1 antibody immunoprecipitated proteins was performed by BGI genomics as previously described⁴⁷. Details on the procedures used in these assays are provided below.

Hematoxylin and eosin, immunofluorescence, IHC staining and BiFC assay.

Hematoxylin and eosin, immunofluorescence and IHC staining were conducted as previously reported⁴⁸. Images of stained sections were captured using the Aperio ScanScope slide scanner (Leica Microsystems). Quantitative analysis and relative score standard of immunostained images were performed with Aperio ImageScope software (Leica Microsystems). Antibody staining area and image intensity were evaluated with the Aperio cytoplasm algorithm (Leica Biosystems), and H scores were calculated by averaging the intensity score for the analyzed region. Upregulation was defined when the cytoplasm H score of the cancer specimen was higher than that of the paired normal one. For coimmunostaining of Gremlin1 and FGFR1 experiments, LNCaP cells were treated with Gremlin1 (100 ng ml⁻¹) alone or in combination with FGF1 (100 ng ml⁻¹) for 10 min at 37 °C before washing and fixation.

For the BiFC experiment, cells transfected with plasmids *GREM1*-VN155 and *FGFR1*-CC155, individually or simultaneously, were plated on cover slides. When cell confluency reached 70% we replaced the culture medium with a basic medium without FBS and allowed cells to grow for a further 12 h. Cells were then kept at 4 °C for 2 h and subsequently washed with ice-cold PBS. Slides were fixed with 4% paraformaldehyde for 30 min at 4 °C and mounted with Vectashield mounting medium (Vector Laboratories). Fluorescent images were captured using a Leica DM2500 microscope.

Protein–protein interaction docking study. Gremlin1 (PDB: 5AEJ) was selected as ligand and FGFR1 (PDB: 3OJV) as receptor for protein–protein docking. The HDock web service was used for docking, with default parameters (<http://hdock.phys.hust.edu.cn/>). Both ligand and receptor protein were first prepared within the Protein Preparation Panel in Schrodinger, with default parameters. Exported PDB files were used for job submission⁴⁹.

PDO culture, PDX and cell line in vivo study. Fresh PCa samples were minced and digested following a reported protocol³¹. Established patient-derived cell lines BM1, BM61, ST88 and ST60 were cultured as previously described³¹. Patient-derived PDX MDA PCa 118b was kept and passaged as previously described³². All patient-derived cells were cultured in culture medium specific for human PCa organoids⁵⁰. For patient-derived PDX experiments, 1 million cells mixed 1:1 with Matrigel (Corning), or tissues in small pieces, were injected or implanted subcutaneously (s.c.) into SCID mice. We started drug treatment when tumor volume reached approximately 200 mm³. Gremlin1 or IgG antibody was dissolved in PBS and administered i.p. at 10 mg kg⁻¹ three times per week for 2 weeks.

1 × 10⁶ PC3 control or PC3 sgFGFR1 cells were suspended in a volume of 50 μl of basic medium and then mixed with Matrigel at a ratio of 1:1. Cell suspensions were injected s.c. into the flanks of BALB/C nude mice (4 weeks old, male; SLAC). Tumor volume was measured three times per week from 1 week post implantation. We used the following formula to calculate tumor volume: tumor volume = (tumor length × width²)/2. Gremlin1 antibody or IgG was injected i.p. three times per week at 10 mg kg⁻¹ for 2 weeks when tumor volume reached 100 mm³. Mice were sacrificed at about 30 days after implantation, when tumors were collected and photographed. All animal experiments were conducted according to the protocols approved by Ren Ji Hospital's committee on animal care. All animals were sacrificed before 20% body weight loss had occurred.

RNA extraction and reverse transcription–qPCR. Total RNA of human prostate tumor samples, adjacent normal tissues and PCa cell lines was extracted by TRIzol

reagent (Invitrogen) according to the manufacturer's protocol. RNA was reverse transcribed into cDNA using the PrimeScript™ RT Reagent Kit (TaKaRa). qPCR was performed using the SYBR Green PCR kit (TaKaRa). β -Actin or GAPDH was used as the internal control gene. All results were calculated by the $\Delta\Delta$ ct method and performed in triplicate. Primers used in the study are listed in Supplementary Table 1.

Immunoblotting, coimmunoprecipitation, pulldown assays and ChIP assay. Immunoblotting experiments were performed using conventional methods. Details of antibodies used in this study are provided in Supplementary Table 2.

For coimmunoprecipitation experiments with endogenous proteins, LNCaP or 293T cells were washed twice with ice-cold PBS and fully lysed in M-PER Mammalian Protein Extraction Reagent (Thermo). For coimmunoprecipitation of exogenous, truncated or mutated proteins, cells were transfected with the indicated plasmids 48 h before harvest and lysis. Cell lysates were mixed with rabbit IgG (abclonal), mouse IgG (abclonal) or the indicated antibody at 4°C overnight. Protein G Agarose beads (Roche) were then added with further incubation for 2 h. The beads were washed twice with HNTG buffer (50 mM HEPES pH 7.4, 150 mM NaCl, 10% glycerol, 1% Triton X-100) supplemented with protease inhibitor. Immunoprecipitates were boiled for 10 min at 98°C in protein loading buffer (Beyotime) for further immunoblotting analysis. Information on antibodies used in coimmunoprecipitation experiments is provided in Supplementary Table 2.

Protein pulldown was performed using purified his-tagged Gremlin1 protein (ACRO Biosystems) and recombinant human FGFR1 beta (IIIc) Fc Chimera protein (R&D). Gremlin1-his protein was enriched using Ni Sepharose 6Fast Flow (GE) following the manufacturer's instructions. FGFR1-Fc protein was enriched by Pierce Protein A/G Magnetic Beads (Thermo). Pulled-down proteins were detected by immunoblotting.

For each ChIP assay, LNCaP or VCaP cells were cultured in 5% charcoal/dextran-stripped FBS medium for 3 days and subsequently treated with DHT at varying concentration, with 1×10^7 cells harvested. The SimpleChIP Enzymatic Chromatin IP Kit (Magnetic Beads; CST) was used following the manufacturer's protocol. The *GREMI* promoter sequence was analyzed using JASPAR (<http://jaspar.genereg.net/>) software to search for androgen response elements. BLAST (blast.ncbi.nlm.nih.gov/Blast.cgi) was utilized to design qPCR primers for AR enrichment analysis. Details of primers used are provided in Supplementary Table 1.

Sphere and cell proliferation assays and Annexin V staining. Single PCa cells (*GREMI* overexpression sublines, *GREMI* knockdown sublines, PC3 or LNCaP cells following the indicated treatment) were suspended in prostate sphere culture medium (DMEM/F12 medium supplemented with N2 (Gibco), B27 (Gibco), epidermal growth factor (PeproTech) and fibroblast growth factor (20 ng ml^{-1} , PeproTech). Cells were seeded in 24-well, low-attachment dishes (Corning) at 1,000 cells per well in 500 μl . Sphere number was counted under a light microscope after 2 weeks.

Cell proliferation assay was performed with cell counting kit-8 (Dojindo). Cells were plated in 96-well plates at 1,000 cells per well and cultured under the indicated treatment condition. Cell proliferation was examined at 24, 48 and 72 h according to the manufacturer's instructions.

Cell apoptosis was accessed by Annexin V-APC (eBioscience) and DAPI (Sigma) staining. Data were collected using a BD Fortessa Flow cytometer and analyzed with Flowjo software.

ELISA and ForteBio assay. For specific binding assays of DAN family proteins, high-binding, clear polystyrene, 96-well plates (Nunc) were coated with 100 μl per well of $2 \mu\text{g ml}^{-1}$ FGFR1-his (Sino biological) in high-pH coating buffer (PBS containing 0.16% Na_2CO_3 and 0.3% NaHCO_3 , pH 9.8) and incubated at 4°C overnight. After three washes with washing buffer (PBS containing 0.1% Tween-20) on an automatic plate washer, 200 μl of blocking buffer (PBS containing 1% BSA, 1% normal goat serum and 0.05% Tween-20) was added to each well and plates were incubated for 2 h at room temperature. DAN family proteins (Gremlin1, DAN, Gremlin2 and COCO) (Sino Biological) were labeled with biotin using the Biotin Antibody Labeling Kit (Novus). Serially diluted biotinylated DAN family proteins (0.0001 – $2.0 \mu\text{g ml}^{-1}$) were applied to wells with incubation at room temperature for 1 h. After a thorough wash, 100 μl of NeutrAvidin (Thermo), diluted in blocking solution at 1:5,000, was then added to the plates with incubation at room temperature for 1 h. Finally, 100 μl per well of 3,3',5,5'-tetramethylbenzidine (TMB; A:B = 1:1) was added to each well and the reaction terminated using $0.64 \text{ M H}_2\text{SO}_4$. The plates were read on a Thermo Multiscan FC at 450 nm.

For confirmation of anti-Gremlin1 specificity, ELISA plates were coated with 100 μl per well of $0.5 \mu\text{g ml}^{-1}$ Gremlin1-his (ACRO Biosystems) or DAN family proteins, with incubation overnight at 4°C. Next, 100 μl of serially diluted anti-human-Gremlin1, anti-murine Gremlin1 or control IgG (0.0001 – $2.0 \mu\text{g ml}^{-1}$) was transferred to wells of the ELISA plates and allowed to incubate for 1 h at room temperature. This was followed by the addition to each well of 100 μl of a solution of horseradish peroxidase conjugated goat anti-mouse IgG and anti-human IgG antibody (Southern Biotech) diluted in blocking solution. Finally, 100 μl per well

of TMB was added to each well. The reaction was terminated and the plates were detected following the methods described above.

For the competing assay of soluble FGFR1, 100 μl per well of $2 \mu\text{g ml}^{-1}$ anti-hFc (ACRO Biosystems) was coated on ELISA plates and the plates incubated for 1 h. After washing and blocking, 100 μl of FGFR1-Fc was applied to the plates at $0.2 \mu\text{g ml}^{-1}$ per well at room temperature for 1 h. Mixtures of Gremlin1 and soluble FGFR1 (50 μl of serially diluted FGFR1-Fc (0.0001 – $20 \mu\text{g ml}^{-1}$) and 50 μl of Gremlin1-biotin ($5 \mu\text{g ml}^{-1}$) were incubated at room temperature for 1 h before being added to the plates. These mixtures were then transferred to wells and allowed to incubate for 1 h at room temperature. The plates were incubated with NeutrAvidin-HRP and detected by TMB, using the protocols mentioned above.

Interaction of Gremlin1 with FGFR1 was evaluated by surface plasmon resonance (ForteBio). Human Gremlin1-his (PeproTech) protein was diluted with kinetics buffer to $2 \mu\text{g ml}^{-1}$. Gremlin1 was immobilized onto a NTA biosensor. The baseline was detected for 60 s, then FGFR1 association was detected for 120 s to acquire K_{on} factor data followed by dissociation in kinetic buffer for 60 s to acquire K_{off} factor data. All kinetics data were collected at 30°C. Data were acquired using the ForteBio Octet RED96 and analyzed using Octet Data Analysis software.

For the FGFR1–Gremlin1 competing assay performed by ForteBio, 100 μl per well of FGFR1-his (Sino biological) at $5 \mu\text{g ml}^{-1}$ was added to the loading column of the plate. Human Gremlin1-Fc (ACRO Biosystems) and FGFR1 (ACRO Biosystems) were diluted with kinetics buffer (PBS pH 7.4, containing 0.1% bovine serum albumin and 0.2% Tween-20) to achieve a concentration of 500 nM in the association column of a 96-well, half-area Microplate (Greiner Bio-one) at 100 μl per well. A mixture of Gremlin1-Fc and FGFR1 at 500 nM was also added to the association column. Kinetics buffer was used as a reference control. NTA sensors were settled in the first baseline column for 60 s to acquire the first baseline. Next, these sensors were placed in the loading column for 120 s to capture the Gremlin1 antibody and then in the second baseline column for 60 s for the second baseline. The NTA sensors were then placed in the association column for 300 s to ensure that protein–protein association was complete. Finally, the sensors were placed in the dissociation column for 100 s. Data were acquired and analyzed as above.

For the assessment of Gremlin1 or FGF1 concentration in prostatic fluid, the human Gremlin1 ELISA kit (LifeSpan BioSciences, no. LS-F6538) and human FGF1 ELISA kit (Boster Biosciences, no. EK0339) were used following the manufacturers' instructions.

Statistical analysis and reproducibility. All statistical analyses were performed with GraphPad 7.0 software. Student's *t*-test assuming equal variance was used, and two-way analysis of variance for independent variance. $P < 0.05$ was considered significant. Data distribution was assumed to be normal, but this was not formally tested. No data were excluded from the analyses. No statistical methods were used to predetermine sample sizes, but ours are similar to those reported in previous publications⁵¹. All animals were randomized and exposed to the same environment. Blinding was not performed in tumor measurement and IHC staining. Treatments or stimuli organized in regard to cells were all randomized. Human specimens were obtained from the Department of Pathology, Ren Ji Hospital by certified pathologists who were blinded to the experiments. Immunoblotting experiments were repeated at least three times, and representative images are shown. Further information on research design is available in the Nature Research Reporting Summary linked to this article.

Reporting summary. Further information on research design is available in the Nature Research Reporting Summary linked to this article.

Data availability

Anti-human Gremlin1 antibody and anti-mouse Gremlin1 antibody were generated in this study. Deep-sequencing (ChIP-seq and RNA-seq) data that support the findings of this study have been deposited in the National Omics Data Encyclopedia, with accession number OEP001758. Previously published microarray data that were reanalyzed here are available at www.oncoPrint.org. The human PCa transcriptome data that support the findings of this study are available at www.cbioportal.com. The data from Beltran et al. generated for this study are available through dbGaP phs000909 and can be accessed by agreement. Source data for Figs. 1–7 and Extended Data Figs. 1–10 have been provided as Source Data files. All other data supporting the findings of this study are available from the corresponding author on reasonable request. Source data are provided with this paper.

Received: 18 March 2021; Accepted: 20 April 2022;

Published online: 27 May 2022

References

- Bray, F. et al. Global cancer statistics 2018: GLOBOCAN estimates of incidence and mortality worldwide for 36 cancers in 185 countries. *CA Cancer J. Clin.* **68**, 394–424 (2018).
- Taylor, B. S. et al. Integrative genomic profiling of human prostate cancer. *Cancer Cell* **18**, 11–22 (2010).

3. Scher, H. I. et al. Increased survival with enzalutamide in prostate cancer after chemotherapy. *N. Engl. J. Med.* **367**, 1187–1197 (2012).
4. Ryan, C. J. et al. Abiraterone in metastatic prostate cancer without previous chemotherapy. *N. Engl. J. Med.* **368**, 138–148 (2013).
5. Tran, C. et al. Development of a second-generation antiandrogen for treatment of advanced prostate cancer. *Science* **324**, 787–790 (2009).
6. Davies, A. H., Beltran, H. & Zoubeidi, A. Cellular plasticity and the neuroendocrine phenotype in prostate cancer. *Nat. Rev. Urol.* **15**, 271–286 (2018).
7. Hsu, D. R., Economides, A. N., Wang, X., Eimon, P. M. & Harland, R. M. The Xenopus dorsalizing factor Gremlin identifies a novel family of secreted proteins that antagonize BMP activities. *Mol. Cell* **1**, 673–683 (1998).
8. Verheyden, J. M. & Sun, X. An Fgf/Gremlin inhibitory feedback loop triggers termination of limb bud outgrowth. *Nature* **454**, 638–641 (2008).
9. Benazet, J. D. et al. A self-regulatory system of interlinked signaling feedback loops controls mouse limb patterning. *Science* **323**, 1050–1053 (2009).
10. Costello, C. M., Cahill, E., Martin, F., Gaine, S. & McLoughlin, P. Role of gremlin in the lung: development and disease. *Am. J. Respir. Cell Mol. Biol.* **42**, 517–523 (2010).
11. Boers, W. et al. Transcriptional profiling reveals novel markers of liver fibrogenesis: Gremlin and insulin-like growth factor-binding proteins. *J. Biol. Chem.* **281**, 16289–16295 (2006).
12. Yan, K. et al. Glioma cancer stem cells secrete Gremlin1 to promote their maintenance within the tumor hierarchy. *Genes Dev.* **28**, 1085–1100 (2014).
13. Davis, H. et al. Aberrant epithelial GREM1 expression initiates colonic tumorigenesis from cells outside the stem cell niche. *Nat. Med.* **21**, 62–70 (2015).
14. Myllarniemi, M. et al. Gremlin-mediated decrease in bone morphogenetic protein signaling promotes pulmonary fibrosis. *Am. J. Respir. Crit. Care Med.* **177**, 321–329 (2008).
15. Carter, P. J. & Lazar, G. A. Next generation antibody drugs: pursuit of the 'high-hanging fruit'. *Nat. Rev. Drug Discov.* **17**, 197–223 (2018).
16. Best, C. J. et al. Molecular alterations in primary prostate cancer after androgen ablation therapy. *Clin. Cancer Res.* **11**, 6823–6834 (2005).
17. Yu, Y. P. et al. Gene expression alterations in prostate cancer predicting tumor aggression and preceding development of malignancy. *J. Clin. Oncol.* **22**, 2790–2799 (2004).
18. Beltran, H. et al. Divergent clonal evolution of castration-resistant neuroendocrine prostate cancer. *Nat. Med.* **22**, 298–305 (2016).
19. Bluemn, E. G. et al. Androgen receptor pathway-independent prostate cancer is sustained through FGF signaling. *Cancer Cell* **32**, 474–489 (2017).
20. Su, W. et al. The Polycomb Repressor Complex 1 drives double-negative prostate cancer metastasis by coordinating stemness and immune suppression. *Cancer Cell* **36**, 139–155 (2019).
21. Abida, W. et al. Genomic correlates of clinical outcome in advanced prostate cancer. *Proc. Natl Acad. Sci. USA* **116**, 11428–11436 (2019).
22. Bennett, J. T. et al. Mosaic activating mutations in FGFR1 cause encephalocraniocutaneous lipomatosis. *Am. J. Hum. Genet.* **98**, 579–587 (2016).
23. Plotnikov, A. N., Hubbard, S. R., Schlessinger, J. & Mohammadi, M. Crystal structures of two FGF-FGFR complexes reveal the determinants of ligand-receptor specificity. *Cell* **101**, 413–424 (2000).
24. Hou, J. et al. Substitution of putative half-cystine residues in heparin-binding fibroblast growth factor receptors. Loss of binding activity in both two and three loop isoforms. *J. Biol. Chem.* **267**, 17804–17808 (1992).
25. Koika, V. et al. Comparative functional analysis of two fibroblast growth factor receptor 1 (FGFR1) mutations affecting the same residue (R254W and R254Q) in isolated hypogonadotropic hypogonadism (IHH). *Gene* **516**, 146–151 (2013).
26. Raivio, T. et al. Impaired fibroblast growth factor receptor 1 signaling as a cause of normosmic idiopathic hypogonadotropic hypogonadism. *J. Clin. Endocrinol. Metab.* **94**, 4380–4390 (2009).
27. Kisonaitte, M., Wang, X. & Hyvonen, M. Structure of Gremlin-1 and analysis of its interaction with BMP-2. *Biochem. J.* **473**, 1593–1604 (2016).
28. Beenken, A., Eliseenkova, A. V., Ibrahim, O. A., Olsen, S. K. & Mohammadi, M. Plasticity in interactions of fibroblast growth factor 1 (FGF1) N terminus with FGF receptors underlies promiscuity of FGF1. *J. Biol. Chem.* **287**, 3067–3078 (2012).
29. Chen, Z. et al. Crucial role of p53-dependent cellular senescence in suppression of Pten-deficient tumorigenesis. *Nature* **436**, 725–730 (2005).
30. Lunardi, A. et al. A co-clinical approach identifies mechanisms and potential therapies for androgen deprivation resistance in prostate cancer. *Nat. Genet.* **45**, 747–755 (2013).
31. Gao, D. et al. Organoid cultures derived from patients with advanced prostate cancer. *Cell* **159**, 176–187 (2014).
32. Li, Z. G. et al. Androgen receptor-negative human prostate cancer cells induce osteogenesis in mice through FGF9-mediated mechanisms. *J. Clin. Invest.* **118**, 2697–2710 (2008).
33. Cappellen, D. et al. Frequent activating mutations of FGFR3 in human bladder and cervix carcinomas. *Nat. Genet.* **23**, 18–20 (1999).
34. Deng, N. et al. A comprehensive survey of genomic alterations in gastric cancer reveals systematic patterns of molecular exclusivity and co-occurrence among distinct therapeutic targets. *Gut* **61**, 673–684 (2012).
35. Weiss, J. et al. Frequent and focal FGFR1 amplification associates with therapeutically tractable FGFR1 dependency in squamous cell lung cancer. *Sci. Transl. Med.* **2**, 62ra93 (2010).
36. Formisano, L. et al. Aberrant FGFR signaling mediates resistance to CDK4/6 inhibitors in ER+ breast cancer. *Nat. Commun.* **10**, 1373 (2019).
37. Ku, S. Y. et al. Rb1 and Trp53 cooperate to suppress prostate cancer lineage plasticity, metastasis, and antiandrogen resistance. *Science* **355**, 78–83 (2017).
38. Mu, P. et al. SOX2 promotes lineage plasticity and antiandrogen resistance in TP53- and RB1-deficient prostate cancer. *Science* **355**, 84–88 (2017).
39. Zou, M. et al. Transdifferentiation as a mechanism of treatment resistance in a mouse model of castration-resistant prostate cancer. *Cancer Discov.* **7**, 736–749 (2017).
40. Labrecque, M. P. et al. Molecular profiling stratifies diverse phenotypes of treatment-refractory metastatic castration-resistant prostate cancer. *J. Clin. Invest.* **129**, 4492–4505 (2019).
41. Bishop, J. L. et al. The master neural transcription factor BRN2 is an androgen receptor-suppressed driver of neuroendocrine differentiation in prostate cancer. *Cancer Discov.* **7**, 54–71 (2017).
42. Svensson, C. et al. REST mediates androgen receptor actions on gene repression and predicts early recurrence of prostate cancer. *Nucleic Acids Res.* **42**, 999–1015 (2014).
43. Worthley, D. L. et al. Gremlin 1 identifies a skeletal stem cell with bone, cartilage, and reticular stromal potential. *Cell* **160**, 269–284 (2015).
44. Quante, M. et al. Bone marrow-derived myofibroblasts contribute to the mesenchymal stem cell niche and promote tumor growth. *Cancer Cell* **19**, 257–272 (2011).
45. Rowan, S. C. et al. Gremlin 1 depletion in vivo causes severe enteropathy and bone marrow failure. *J. Pathol.* **251**, 117–122 (2020).
46. Hieronymus, H. et al. Gene expression signature-based chemical genomic prediction identifies a novel class of HSP90 pathway modulators. *Cancer Cell* **10**, 321–330 (2006).
47. Zhu, X. et al. Ubiquitination of inositol-requiring enzyme 1 (IRE1) by the E3 ligase CHIP mediates the IRE1/TRAF2/JNK pathway. *J. Biol. Chem.* **289**, 30567–30577 (2014).
48. Zhou, Z. et al. TRIM59 is up-regulated in gastric tumors, promoting ubiquitination and degradation of p53. *Gastroenterology* **147**, 1043–1054 (2014).
49. Yan, Y., Zhang, D., Zhou, P., Li, B. & Huang, S. Y. HDOCK: a web server for protein-protein and protein-DNA/RNA docking based on a hybrid strategy. *Nucleic Acids Res.* **45**, W365–W373 (2017).
50. Drost, J. et al. Organoid culture systems for prostate epithelial and cancer tissue. *Nat. Protoc.* **11**, 347–358 (2016).
51. Zhang, K. et al. WNT/beta-catenin directs self-renewal symmetric cell division of hTERT(high) prostate cancer stem cells. *Cancer Res.* **77**, 2534–2547 (2017).

Acknowledgements

The study was supported by funds to H.H.Z. from the National Key R&D Program of China (no. 2017YFA0102900), the National Natural Science Foundation of China (nos. NSFC32022021, and NSFC81972404), the Program of Shanghai Academic/Technology Research Leader (no. 21XD1422300), the Shanghai Municipal Education Commission-Gaofeng Clinical Medicine Grant Support (no. 20181706) and the Innovative research team of high-level local universities in Shanghai; and by funds to W.-Q.G. from NSFC (nos. 81630073 and 81872406), 111 project (no. B21024), the Science and Technology Commission of Shanghai Municipality (nos. 20JC1417600 and 21JC1404100), Peak Disciplines (Type VI) of Institutes of Higher Learning in Shanghai, the Shanghai Jiao Tong University STAR and Scientific and Technological Innovation Funds and the KC Wong foundation. Funding for the generation and production of antibodies for Gremlin1 were provided by Mabspace Biosciences.

Patient-derived organoid lines BMI1, BM61, ST88 and ST60 were kindly provided by Prof. Dong Gao (Shanghai Institute of Biochemistry and Cell Biology, Chinese Academy of Sciences, Shanghai, China). Patient-derived PDX MDA PCA 118b was generously shared by Prof. Nora M. Navone (Department of Genitourinary Medical Oncology) and the David H. Koch Center for Applied Research of Genitourinary Cancers, the University of Texas MD Anderson Cancer Center, Houston, Texas.

Author contributions

H.H.Z. and W.-Q.G. conceived the study. X.Q. contributed to antibody-related study design. C.C. and J.W. performed the experiments. L.F., Y.G., Z.X., B.D. and W.X. collected clinical patient samples. K.Z. provided support for in vivo experiments. D.W., N.J., Z.J., L.F. and H.H.Z. helped with cell culture experiments. Y.H. and Y.G. participated in immunostaining and imaging. P.X., M.Z., K.L. and P.Z. assisted with animal experiments. J.Z. and P.Z. supported data analysis. C.L. provided assistance with ChIP

experiments. B.D. and W.X. provided clinical patient samples, patient-derived cell lines and histological assessment. S.C., Z.S., D.S., X.Y., H.L. and X.Q. provided support for antibody generation, engineering, production and characterization. H.H.Z., W.-Q.G., C.C. and J.W. interpreted the data and wrote the manuscript.

Competing interests

X.Q., Z.S., D.S., X.Y. and H.L. are employees and shareholders of Mabspace Biosciences (Suzhou) Co., Ltd.

Additional information

Extended data is available for this paper at <https://doi.org/10.1038/s43018-022-00380-3>.

Supplementary information The online version contains supplementary material available at <https://doi.org/10.1038/s43018-022-00380-3>.

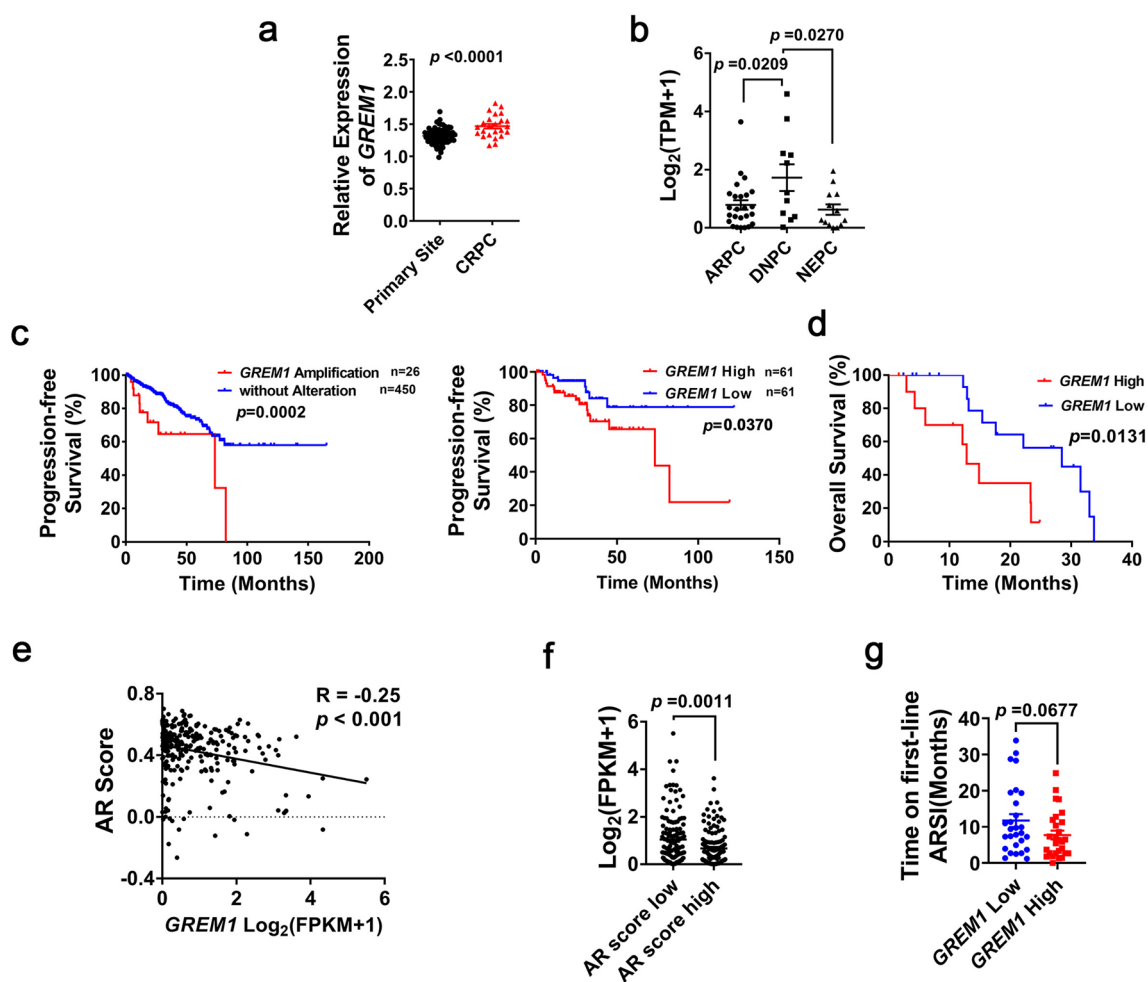
Correspondence and requests for materials should be addressed to Wei-Qiang Gao or Helen He Zhu.

Peer review information *Nature Cancer* thanks Leigh Ellis, John Isaacs and Ping Mu for their contribution to the peer review of this work.

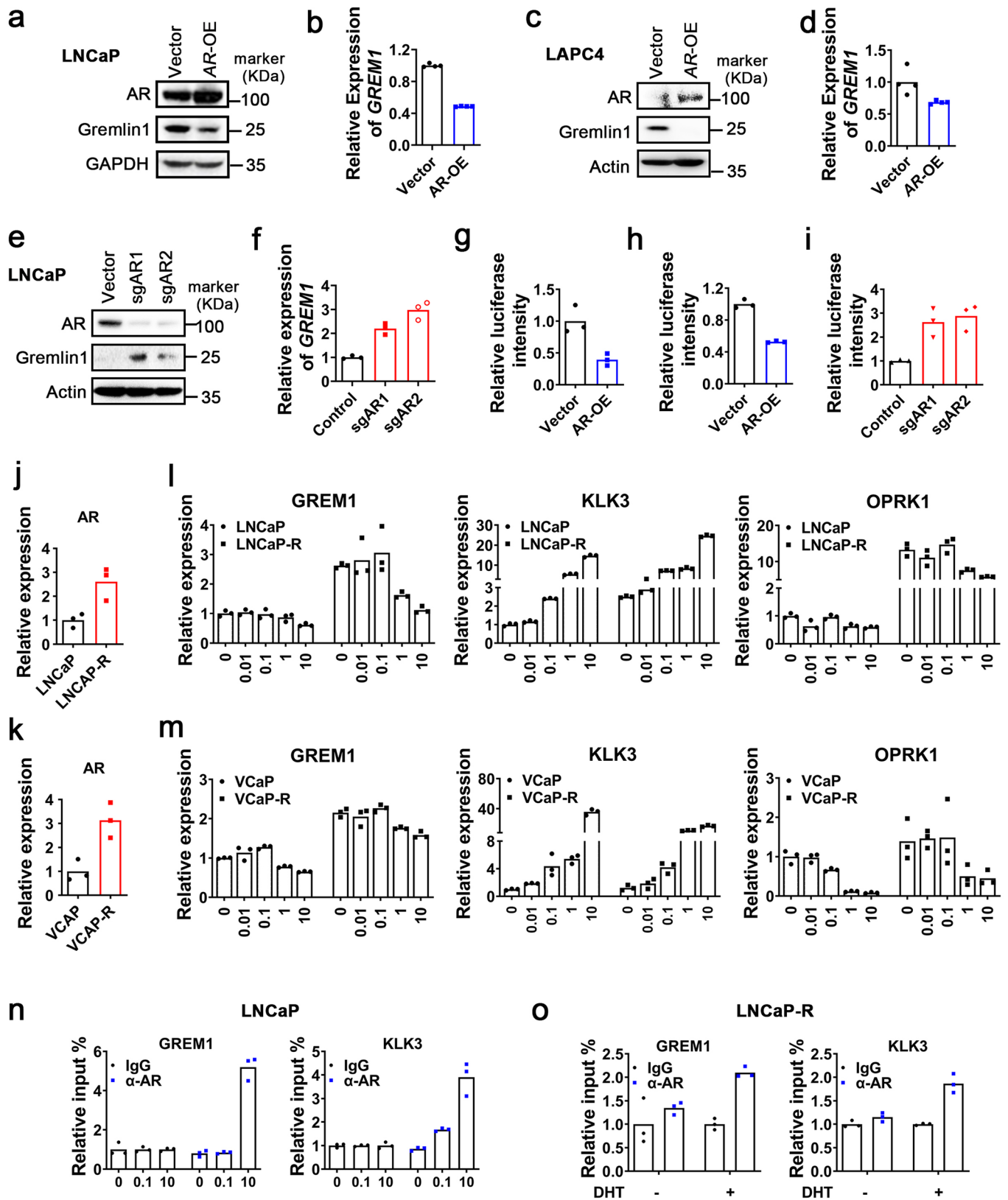
Reprints and permissions information is available at www.nature.com/reprints.

Publisher's note Springer Nature remains neutral with regard to jurisdictional claims in published maps and institutional affiliations.

© The Author(s), under exclusive licence to Springer Nature America, Inc. 2022

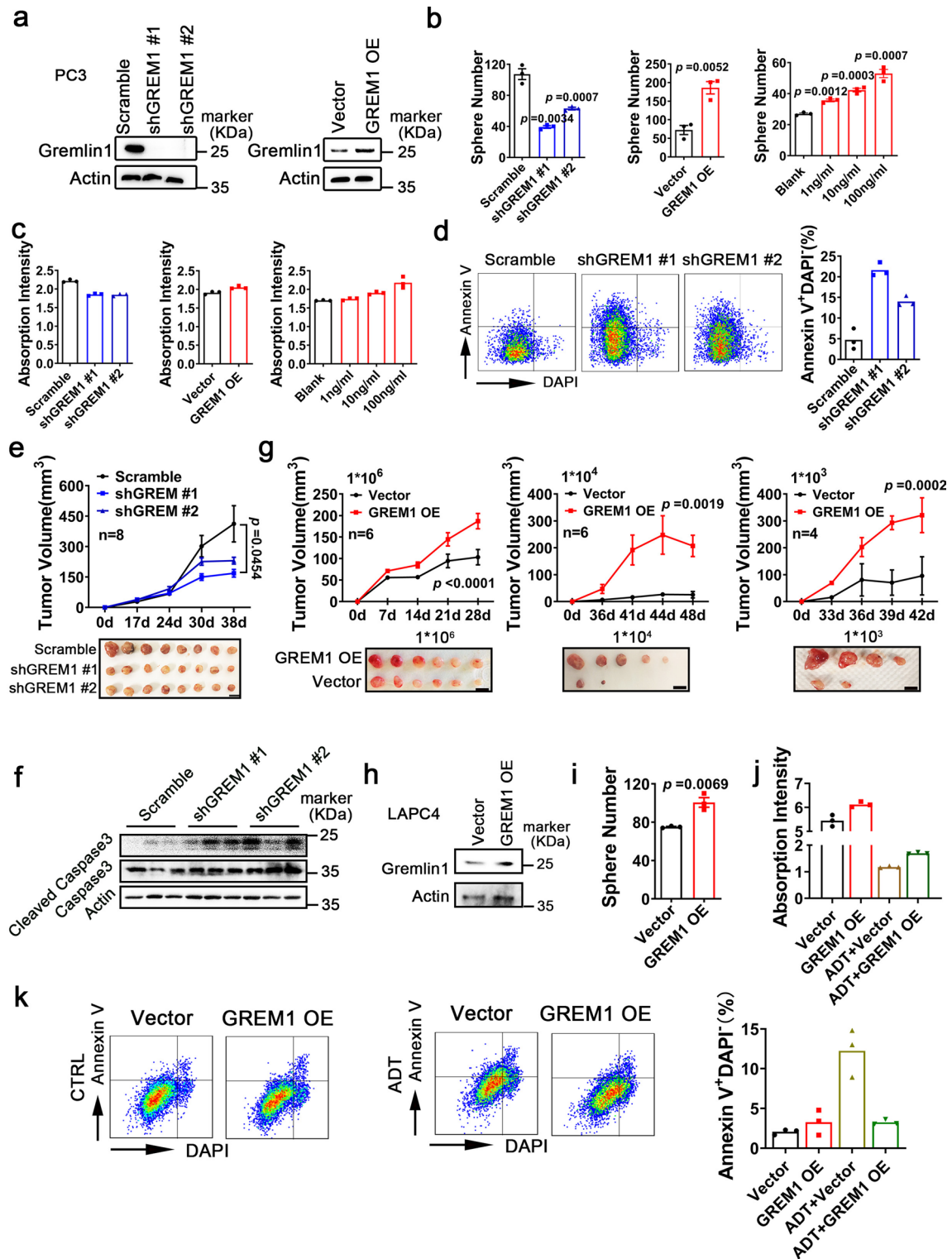


Extended Data Fig. 1 | Gremlin1 is upregulated in CRPCs and associated with a poor disease outcome. (a) Analysis of Oncomine PCa dataset (Yu dataset (GSE6919), $n = 64$ tumor samples in primary site; $n = 24$ CRPC samples) demonstrates that the *GREM1* expression level is significantly upregulated in castration resistant PCa. (b) The *GREM1* gene transcription is significantly upregulated in DNPC (data were obtained from the Beltran 2016 dataset (dbGaP phs000909), $n = 25$ ARPC samples, $n = 11$ DNPC samples, $n = 13$ NEPC samples). (c) A significant shorter disease/progression-free survival time in patients carrying *GREM1* gene copy number amplifications compared to patients without *GREM1* DNA alterations (left panel) or in patients with higher *GREM1* mRNA expression (right panel). (d) High expression of Gremlin1 has a positive correlation with poor overall survival in SU2C 2019 dataset (dbGaP phs000915). (e-f) *GREM1* mRNA exhibits a negative correlation with AR score in the SU2C 2019 dataset, total $n = 266$ tumor samples, $n = 133$ tumor samples in the group of high AR score, $n = 133$ tumor samples in the group of low AR score. The AR score here was acquired from the cBioPortal database which contains 30 AR responsive genes described previously. FPKM, fragments per kilobase million. (g) The treatment time on AR targeted therapy in patient groups with high or low expression level of Gremlin1 in the SU2C 2019 dataset (dbGaP phs000915), $n = 28$ tumor samples in the group of *GREM1* high, $n = 28$ tumor samples in the group of *GREM1* low. (Two-tailed Student's *t* test was used for the statistical analysis. Log-rank (Mantel-Cox) test was used for the survival analysis. Data are presented as means \pm s.e.m.).



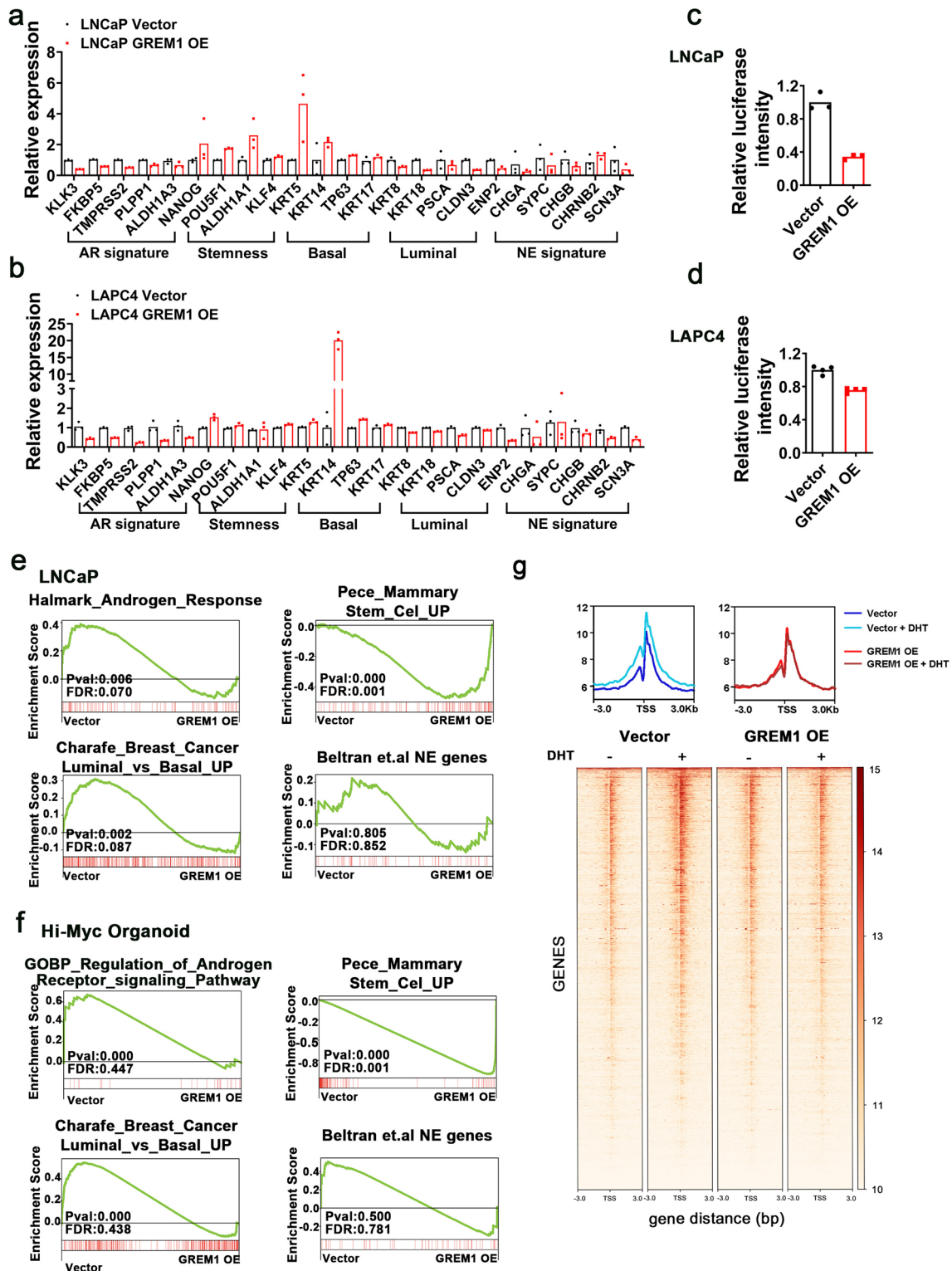
Extended Data Fig. 2 | See next page for caption.

Extended Data Fig. 2 | Transcriptional suppression of AR on *GREM1* depends on a high androgen concentration. (a-i) Immunoblotting and q-PCR analysis of *GREM1* expression, and *GREM1* promoter-driven luciferase assay in AR overexpressed LNCaP (a, b, g) or LAPC4 cells (c, d, h) and AR knock-out LNCaP cells (e, f, i) (b, d, n = 4 independently treated cell cultures, f, n = 3 independently treated cell cultures, g, h, i, n = 3 independently transfected replicates). (j, k) The AR gene transcription is upregulated in LNCaP-R and VCAP cells treated with charcoal/dextran-stripped FBS for 3 weeks (VCAP-R) (n = 3 independently treated cell cultures). (l, m) LNCaP or LNCaP-R cells and VCAP or VCAP-R cells were treated with 0, 0.01, 0.1, 1, or 10 nM DHT for 24 hrs. *GREM1*, *KLK3* and *OPRK1* mRNA are measured by q-PCR analysis (n = 3 independently treated cell cultures). (n) 0, 0.1 or 10 nM DHT were added to LNCaP cells for 4 hr. Binding of AR to the ARE of *GREM1* or *KLK3* gene is measured by ChIP q-PCR. (o) LNCaP-R cells were treated with or without 10 nM DHT. The enrichment of AR to *GREM1* and *KLK3* gene is measured by ChIP q-PCR (n = 3 independently treated cell cultures). (Two-tailed Student's t test was used for the statistical analysis. Data are presented as means \pm s.e.m.).

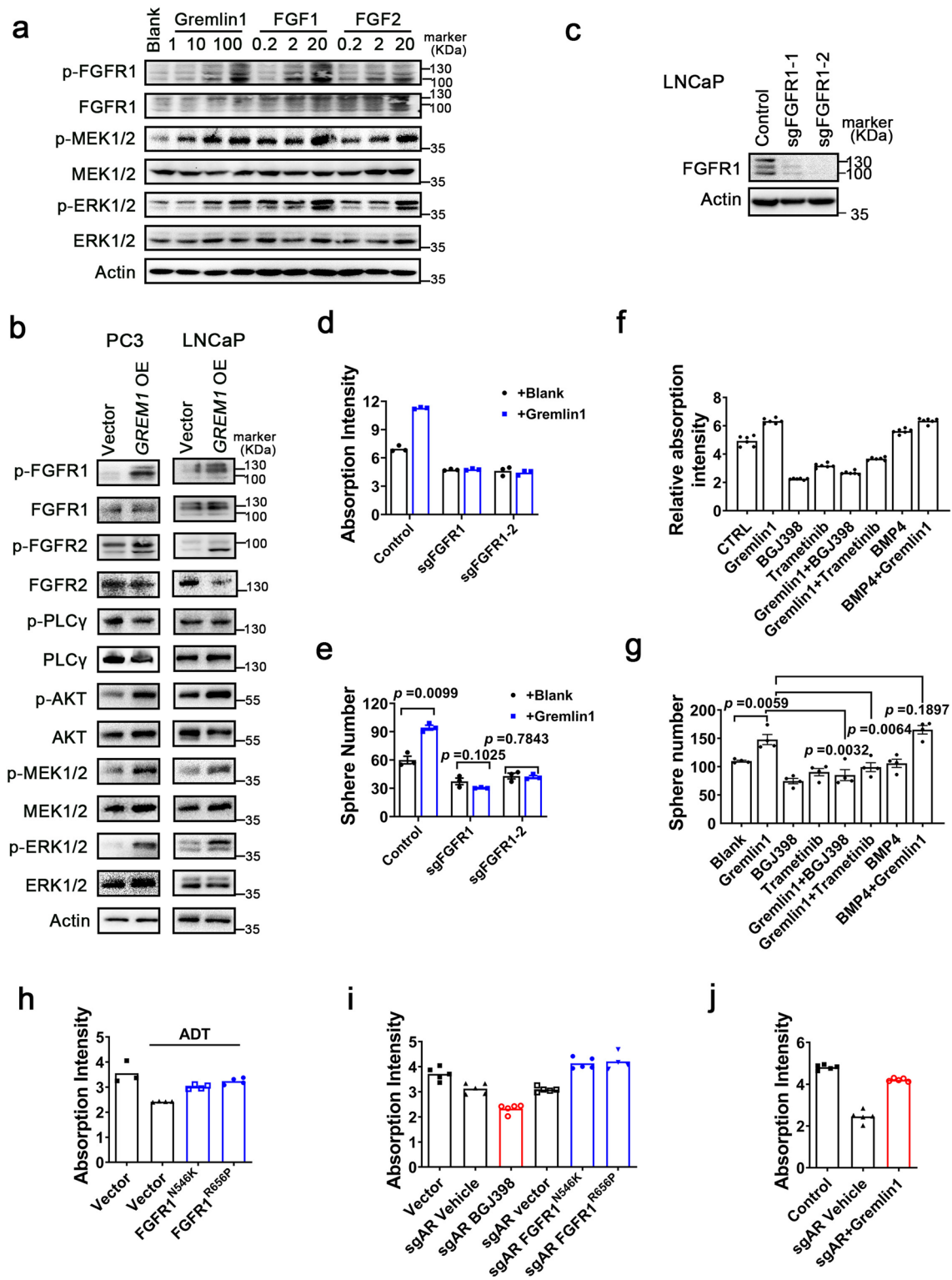


Extended Data Fig. 3 | See next page for caption.

Extended Data Fig. 3 | Gremlin1 promotes PCa cell proliferation, castration resistance and tumor growth in vivo. (a) Immunoblotting confirms the efficiency of *GREM1* knockdown or *GREM1* overexpression in PC3 cells. (b, c) *GREM1* knockdown leads to a suppression of sphere formation capacity ($n=3$ biological replicates) (b) and cell proliferation ($n=3$ independently treated cell cultures) (c) in PC3 cells, while *GREM1* overexpression or addition of exogenous Gremlin1 protein display a promoting effect. (d) Knockdown of *GREM1* increases cell apoptosis in PC3 cells ($n=3$ independently treated cell cultures). (e) *GREM1* knockdown represses PC3 xenografts growth in vivo. $n=8$ mice. (f) *GREM1* knockdown increases cell apoptosis of PC3 xenografts in vivo characterized by the level of cleaved caspase3. (g) *GREM1* overexpression promotes PC3 xenografts forming incidence and tumor growth in vivo. Scale bars = 1 cm. $n=6$ mice in the xenograft experiments with 1×10^6 and 1×10^4 cells. $n=4$ mice in the 1×10^4 cell xenograft assay. (h) Immunoblotting confirms Gremlin1 overexpression in LAPC4 cells transfected with *GREM1* lentivirus. (i) Gremlin1 enhances sphere forming of LAPC4 cells ($n=3$ biological replicates). (j) Gremlin1 promotes the growth of LAPC cells under the ADT treatment ($n=3$ independently treated cell cultures). (k) *GREM1* overexpression prevents cell death upon enzalutamide treatment characterized by a decreased Annexin V/DAPI staining ($n=3$ independently treated cell cultures). Immunoblotting was repeated at least 3 times and representative images were shown. ADT: treated with enzalutamide at $10 \mu\text{g/ml}$. (Two-tailed Student's *t* test was used for the statistical analysis. Two-way ANOVA analysis were used for the measurement of tumor volume. Data are presented as means \pm s.e.m.).

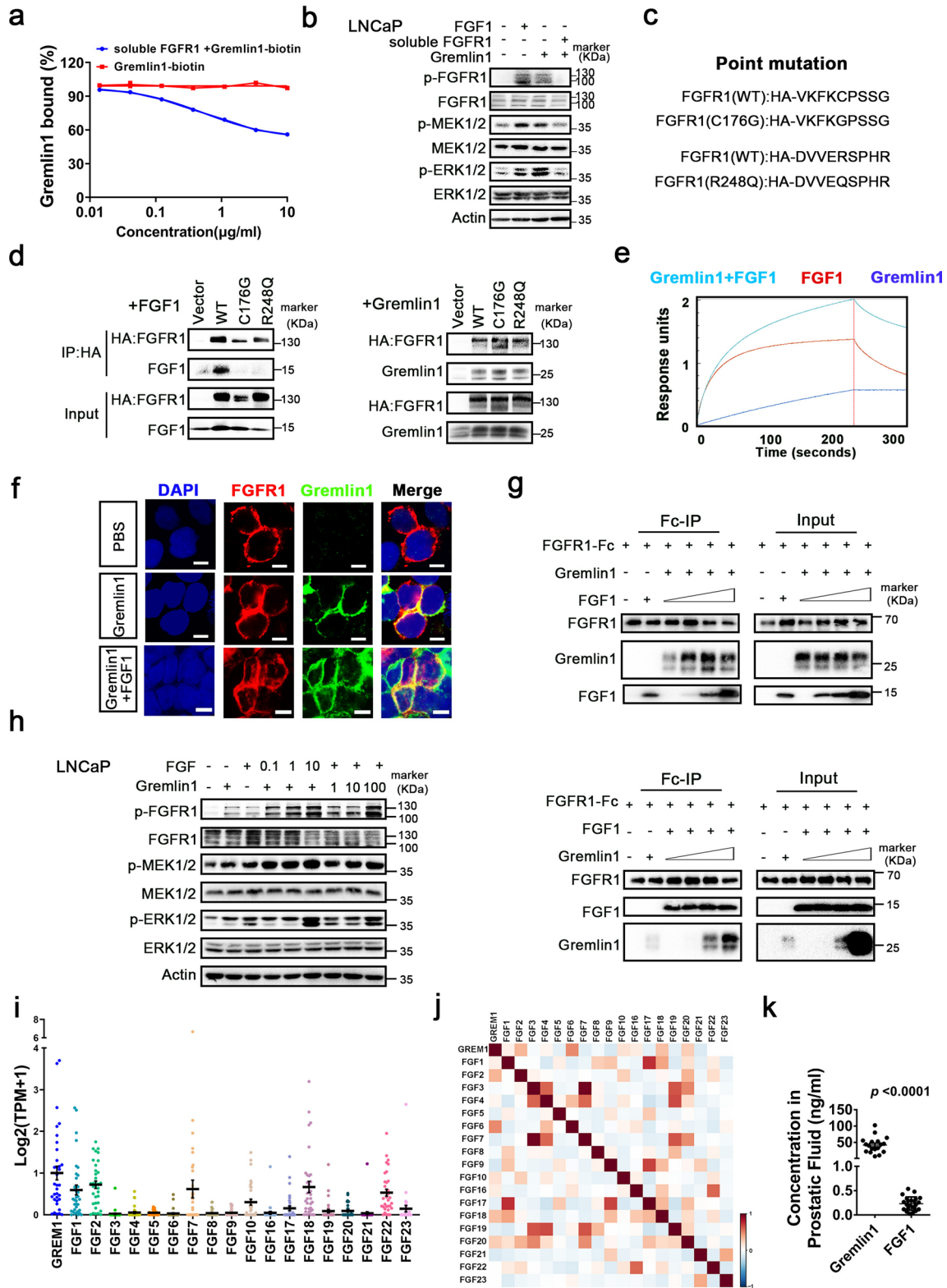


Extended Data Fig. 4 | Gremlin1 induces a decrease in AR signaling and alterations in expression of cell lineage genes in PCa cells. (a, b) q-PCR assessment of transcription of AR signaling genes, stem cell-related genes, basal, luminal, and neuroendocrine lineage makers in control and *GREM1* overexpressing LNCaP (a) or LAPC4 (b) cells ($n=3$ independently treated cell cultures). (c, d) ARE-luciferase reporter assay demonstrates an AR signaling decrease upon *GREM1* overexpression in LNCaP (c) ($n=3$ independently transfected replicates) or LAPC4 (d) cells ($n=4$ independently transfected replicates). (e, f) Gene set enrichment analysis shows a downregulation of AR signaling and luminal genes, and an enrichment of basal cell signature and stemness genes in *Gremlin1* overexpressed LNCaP cells (e) and *Hi-Myc* mouse PCa derived organoids (f) ($n=3$ independent samples). (g) ChIP-seq analysis indicate a reduced AR chromatin binding intensity at AR target genes.



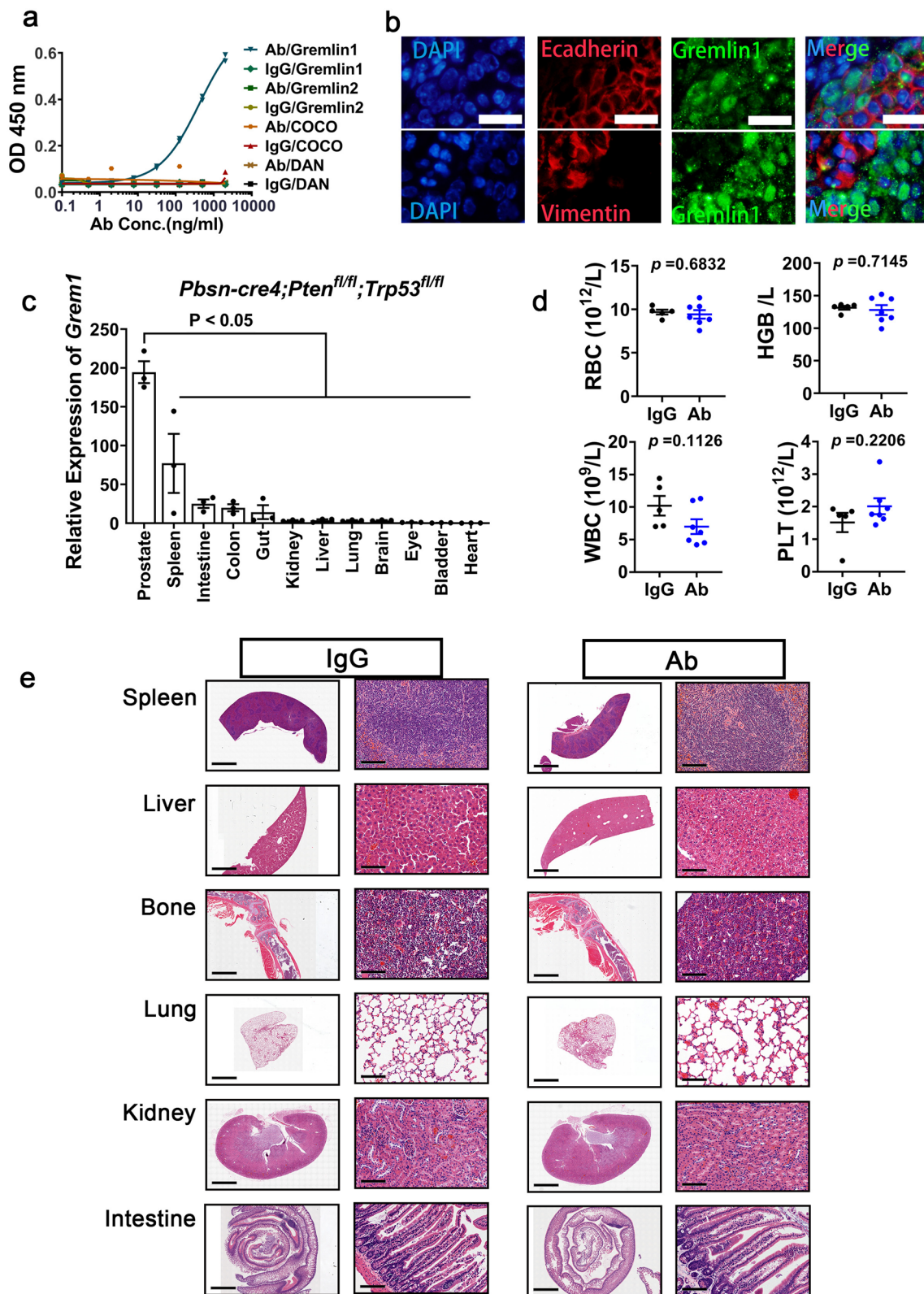
Extended Data Fig. 5 | See next page for caption.

Extended Data Fig. 5 | Gremlin1 promotes PCa in a FGFR1/MAPK-dependent manner. (a) Gremlin1 treatment leads to an activation of FGFR1/MEK/ERK signaling pathway in a dose-dependent way. FGF1 and FGF2 are used as positive controls. Concentration (ng/ml) of Gremlin1, FGF1 and FGF2 are shown in the figure. (b) FGFR1/MEK/ERK signaling pathway is activated in the *GREM1* overexpressed PC3 and LNCaP cells. *GREM1* overexpression also promotes FGFR2 and AKT phosphorylation. (c) Immunoblotting shows the efficiency of FGFR1 knockout in LNCaP cells. (d, e) FGFR1 knockout significantly attenuates the positive effects of Gremlin1 (100 ng/ml) on LNCaP-R cell proliferation ($n = 3$ independently treated cell cultures) and sphere formation ($n = 3$ biological replicates). (f, g) The promoting effects of Gremlin1 protein (100 ng/ml) on LNCaP-R cells proliferation (f, $n = 6$ independently treated cell cultures) and sphere forming (g, $n = 4$ biological replicates) are abrogated by FGFR or MEK inhibitors but are not affected by the addition of BMP4 or BMP6. BGJ398, FGFR1 inhibitor; Trametinib, MEK inhibitor. (h, i) FGFR1 activation promotes LNCaP cell growth in ADT condition (f, $n = 4$ independently treated cell cultures) or upon AR knock-out (g, $n = 5$ independently treated cell cultures). LNCaP or LNCaP sgAR cells were transfected with plasmids expressing FGFR1 N546K or FGFR1 R656P constitutively activated mutation, or treated with FGFR1 inhibitor BGJ398. (j) Addition of Gremlin1 protein enhances the cell proliferation in LNCaP AR knock-out cells ($n = 5$ independently treated cell cultures). Immunoblotting was repeated at least 3 times and representative images were shown. (Two-tailed Student's *t* test was used for the statistical analysis. Data are presented as means \pm s.e.m.).

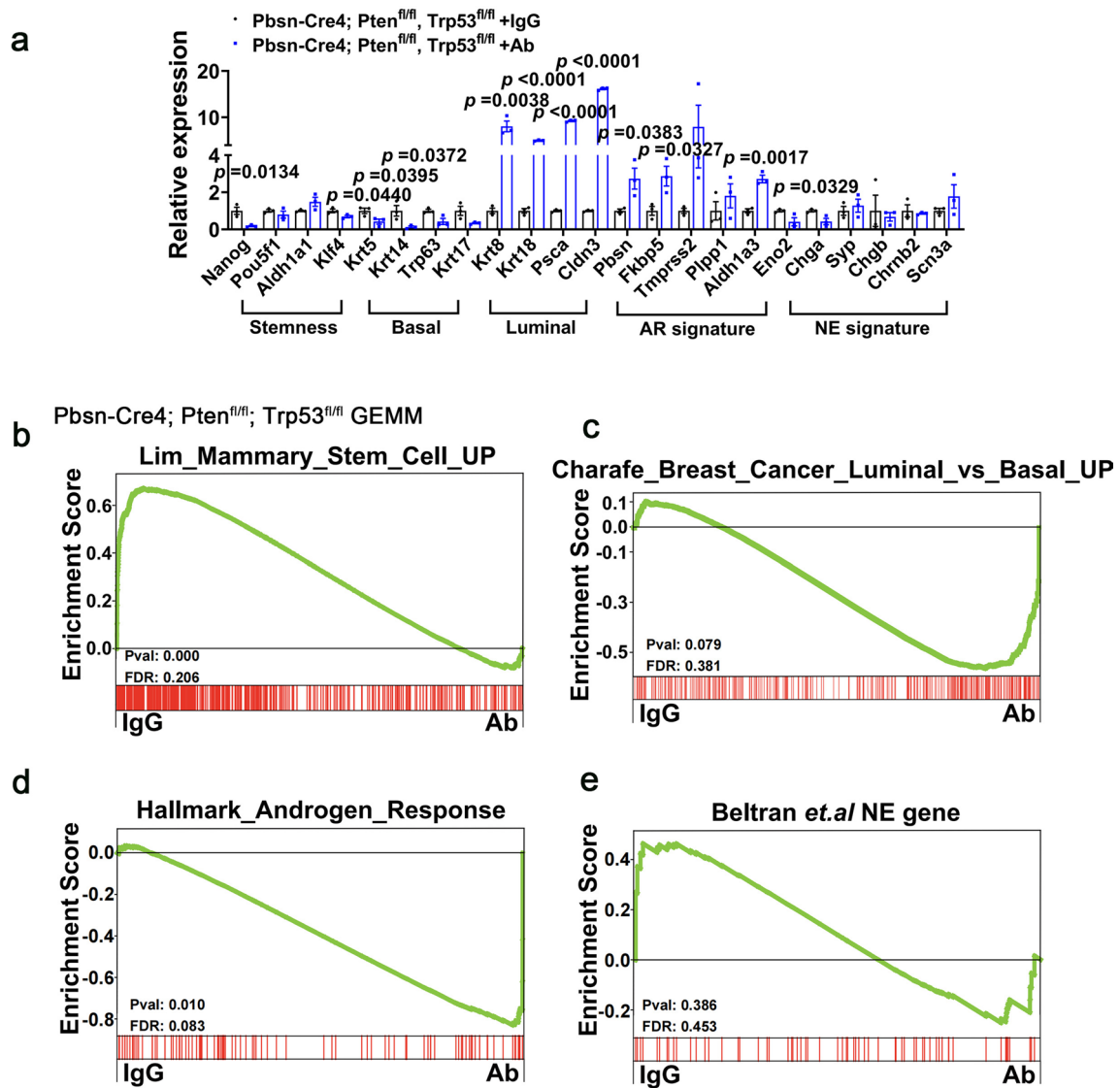


Extended Data Fig. 6 | See next page for caption.

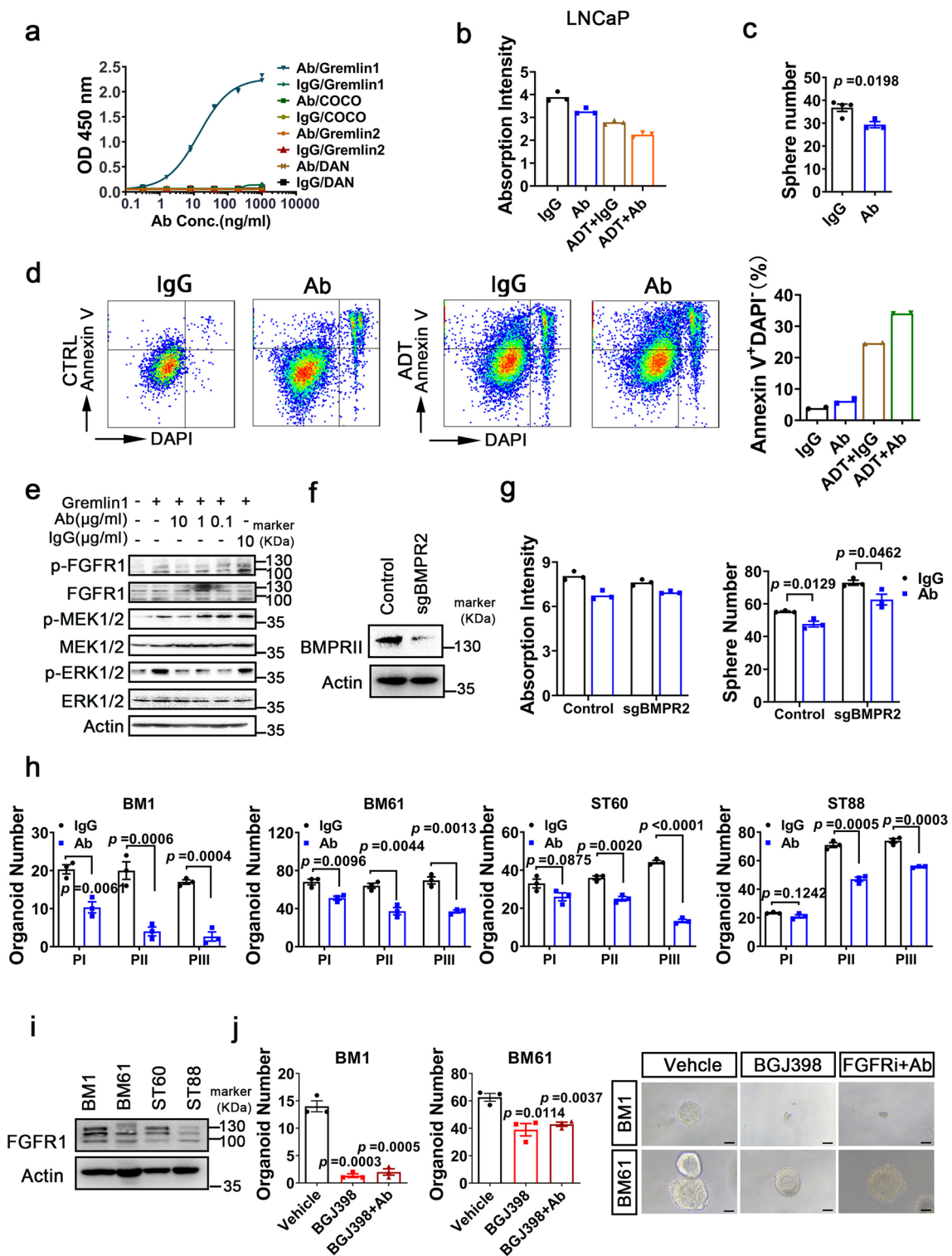
Extended Data Fig. 6 | Gremlin1 binds to FGFR1 in a way different from FGF1/FGFR1 interaction. (a) The specific binding of Gremlin1 to immobilized FGFR1 is competed by soluble FGFR1 in a dose-dependent manner ($n=2$ technical replicates, experiments have been repeated twice). (b) Soluble FGFR1 (200 ng/ml) competitively inhibits the activation of FGFR1/MEK/ERK signaling by Gremlin1 (100 ng/ml) in PC3. The experiments were repeated at least 3 times with similar results. (c) Schematics of FGFR1 mutations. (d) FGFR1-C176G or FGFR1-R248Q mutation abolishes co-immunoprecipitation of FGF1 and FGFR1(left panel), but do not influence the forming of protein complex between Gremlin1 and FGFR1(right panel). The experiments were repeated at least 3 times with similar results. (e-h) The binding between Gremlin1 and FGFR1 is not affected by addition of FGF1, and vice versa, which are revealed by Fortebio (e), co-immunostaining (f), pull-down (g), and immunoblotting (h) assays. Scale bars = 10 μm . The Fortebio experiment was repeated at least twice with similar results. The pull-down and immunoblotting assay were repeated at least 3 times with similar results. The immunostaining experiment was repeated at least twice. Multiple fields of cell culture slides were examined during each repeat and representative images were shown. (i) mRNA levels of *GREM1* and *FGFs* in CRPCs (data were obtained from the Beltran 2016 dataset (dbGaP, phs000909), $n=49$ tumor samples). (j) Correlation analysis of *GREM1* and *FGFs* expression in CRPCs (data were obtained from the Beltran 2016 dataset (dbGaP, phs000909), $n=49$ tumor samples). (k) The concentration of Gremlin1 and FGF1 in prostatic fluid of human PCa patients is analyzed by the enzyme-linked immunosorbent assay. $n=18$ prostatic fluid samples in Gremlin1 ELISA assay; $n=23$ prostatic fluid samples in FGF1 ELISA assay. (Two-tailed Student's *t* test was used for the statistical analysis. Data are presented as means \pm s.e.m.).



Extended Data Fig. 7 | Gremlin1 antibody treatment in mice does not cause major side effects in vivo. (a) Binding specificity of anti-murine Gremlin1 antibody to Gremlin1 is validated by the enzyme-linked immunosorbent assay (n = 2 technical replicates, experiments have been repeated twice). Ab is anti-Gremlin1 in this figure. (b) Gremlin was mainly expressed by the tumorous epithelial cells in castrated *Pbsn-Cre4; Pten^{fl/fl}; Trp53^{fl/fl}* PCa. Scale bars = 20µm. The immunostaining experiment was repeated at least twice. The representative images were presented. (c) *Greml1* was most highly expressed in the prostate cancer tissue compared to other organs from *Pbsn-Cre4; Pten^{fl/fl}; Trp53^{fl/fl}* mice (n = 3 mice). (d, e) Gremlin1 antibody treatment does not induce major side effects when administered systemically to mice (10 mg/kg three times a week). No obvious alterations are detected in peripheral blood cell counts (d, IgG: n = 5 mice; Ab: n = 7 mice) or major organs (e) in mice received the antibody treatment. Scale bars: left panel = 2 mm; right panel = 100 µm. Ab: anti-murine Gremlin1. (Two-tailed Student's t test was used for the statistical analysis. Data are presented as means ± s.e.m.).

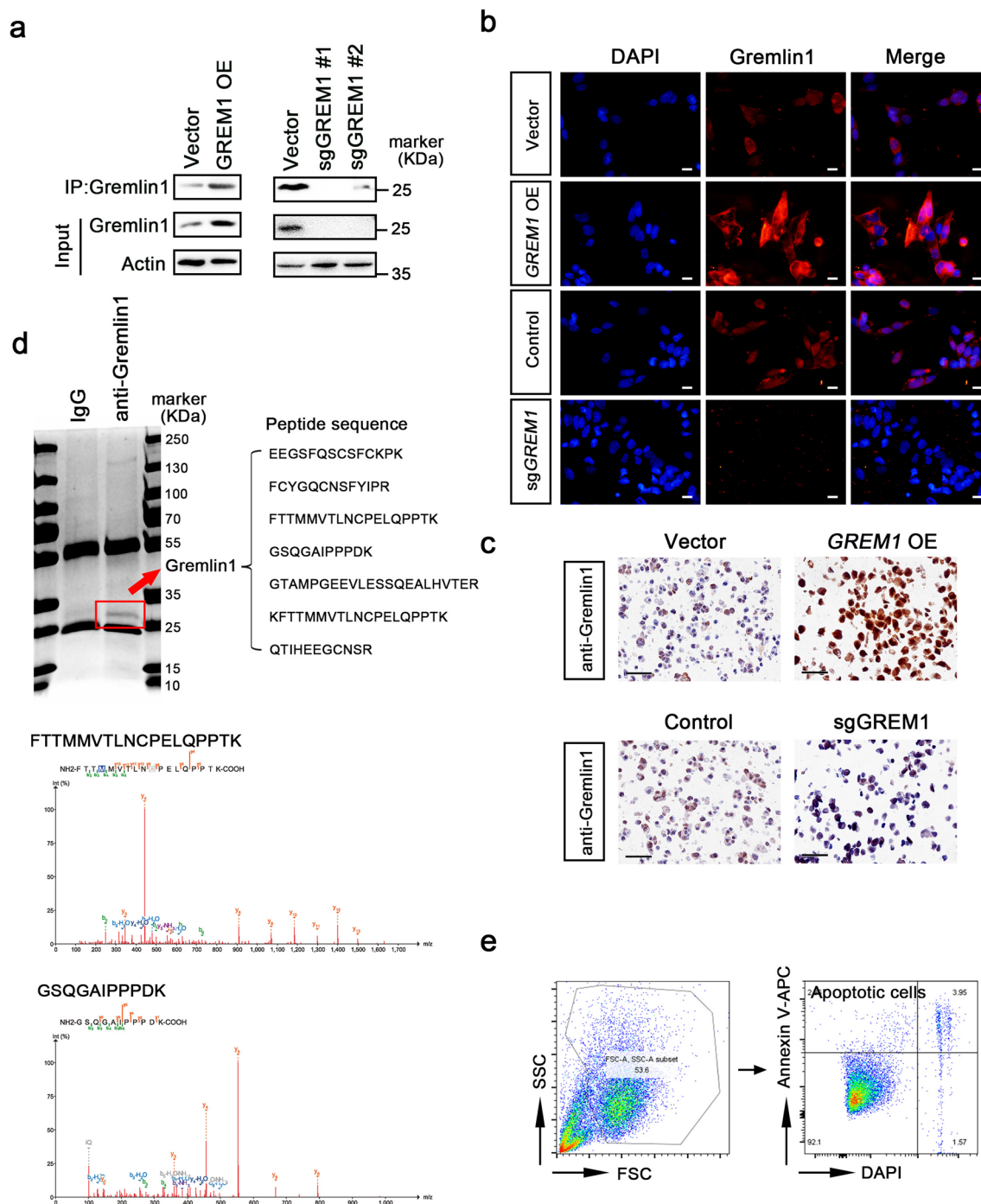


Extended Data Fig. 8 | Gremlin1 antibody treatment suppresses stem cell-related gene expression, whereas upregulates AR signaling and luminal signature genes in murine *Pbsn-Cre4; Pten^{fl/fl}; Trp53^{fl/fl}* PCa. (a-e) q-PCR (a) and Gene set enrichment analysis (b-e) on stem cell-related gene, AR signaling, luminal, basal, and neuroendocrine signatures on anti-Gremlin1 antibody-treated murine *Pbsn-Cre4; Pten^{fl/fl}; Trp53^{fl/fl}* prostate cancer tissue (n=3 mice). FDR, false discovery rate. (Two-tailed Student's t test was used for the statistical analysis. Data are presented as means \pm s.e.m.).



Extended Data Fig. 9 | See next page for caption.

Extended Data Fig. 9 | Antitumor effects of the Gremlin1 antibody are acted through the FGFR1 inhibition. (a) Binding specificity of the anti-human Gremlin1 to Gremlin1 is validated by the enzyme-linked immunosorbent assay. Ab is anti-human Gremlin1 in this figure. (b) The antibody against Gremlin1 (100 ng/ml) facilitates the inhibition of in vitro cell proliferation by enzalutamide (10 μ g/ml) ($n = 3$ independently treated cell cultures). (c) Anti-Gremlin1 treatment suppresses the sphere formation ability of LNCaP-R cells ($n = 3$ biological replicates). (d) Annexin-V/DAPI staining demonstrates that anti-Gremlin1 antibody displays a synergistic effect with enzalutamide in inducing cell death ($n = 2$ independently treated cell cultures, experiments have been repeated at least 3 times). (e) The activation of FGFR1/MEK/ERK signaling pathway is suppressed by the Gremlin1 antibody in LNCaP-R cells. The experiment was repeated at least 3 times with similar results. (f) Immunoblotting confirms the efficiency of *BMPR2* knockout in LNCaP-R cells. The experiment was repeated at least 3 times with similar results. (g) *BMPR2* knockout shows no significant influence to the inhibitory effect of Gremlin1 antibody (10 μ g/ml) on LNCaP-R cell proliferation ($n = 3$ independently treated cell cultures) and sphere formation ($n = 3$ biological replicates). Ab: anti-Gremlin1. ADT: treated with enzalutamide at 10 μ g/ml. (h) Anti-Gremlin1 antibody (10 μ g/ml) suppresses PCa PDO formation in a serial organoid forming assay ($n = 3$ biological replicates). (i) Expression levels of FGFR1 in four patient-derived xenograft lines are assessed by immunoblotting. The experiment was repeated at least 3 times with similar results. (j) FGFR inhibitor BGJ398 decreases organoid forming capacity of BM1 and BM61 PDX lines. No additive effect is detected between BGJ398 (1 μ M) and Gremlin1 antibody (10 μ g/ml) treatment ($n = 3$ biological replicates). Scale bars = 50 μ m. FGFRi, FGFR1 inhibitor BGJ398. (Two-tailed Student's *t* test was used for the statistical analysis and the tumor size at the end timepoint was analyzed. Data are presented as means \pm s.e.m.).



Extended Data Fig. 10 | Validation of the anti-human Gremlin1 antibody for various applications and gating strategy for flow cytometry in this study. (a-c) Antibody specificity of the anti-human Gremlin1 antibody (Mabspace Biosciences) in immunoprecipitation, immunoblotting, IHC and IF was validated using *GREM1* overexpressing, *GREM1* knockout and respective control LNCaP cells. IHC Scale bars = 50 μ m, IF Scale bars = 20 μ m. The immunostaining experiment was repeated at least twice and representative images were presented. The immunoblotting experiment was repeated at least 3 times with similar results. (d) Mass spectrum of immunoprecipitants with the anti-human Gremlin1 antibody (Mabspace Biosciences) in LNCaP cells shows an enrichment of the Gremlin1 protein. The experiment was repeated at least 3 times with similar results. (e) Gating strategy for the flow cytometric examination of apoptosis in this study. The frequency of the cells in the apoptotic stage were calculated based on APC⁺/DAPI⁻.

Reporting Summary

Nature Portfolio wishes to improve the reproducibility of the work that we publish. This form provides structure for consistency and transparency in reporting. For further information on Nature Portfolio policies, see our [Editorial Policies](#) and the [Editorial Policy Checklist](#).

Statistics

For all statistical analyses, confirm that the following items are present in the figure legend, table legend, main text, or Methods section.

n/a Confirmed

- The exact sample size (n) for each experimental group/condition, given as a discrete number and unit of measurement
- A statement on whether measurements were taken from distinct samples or whether the same sample was measured repeatedly
- The statistical test(s) used AND whether they are one- or two-sided
Only common tests should be described solely by name; describe more complex techniques in the Methods section.
- A description of all covariates tested
- A description of any assumptions or corrections, such as tests of normality and adjustment for multiple comparisons
- A full description of the statistical parameters including central tendency (e.g. means) or other basic estimates (e.g. regression coefficient) AND variation (e.g. standard deviation) or associated estimates of uncertainty (e.g. confidence intervals)
- For null hypothesis testing, the test statistic (e.g. F , t , r) with confidence intervals, effect sizes, degrees of freedom and P value noted
Give P values as exact values whenever suitable.
- For Bayesian analysis, information on the choice of priors and Markov chain Monte Carlo settings
- For hierarchical and complex designs, identification of the appropriate level for tests and full reporting of outcomes
- Estimates of effect sizes (e.g. Cohen's d , Pearson's r), indicating how they were calculated

Our web collection on [statistics for biologists](#) contains articles on many of the points above.

Software and code

Policy information about [availability of computer code](#)

Data collection The Beltran dataset was collected with sratools 2.11.0. The others were collected with Microsoft Excel.

Data analysis The Libraries were generated using the NEBNext UltraTM RNA Library Prep Kit for Illumina (NEB) and index codes were added to each sample. Adapters were cutted by Cutadapt (2.6) and clean reads were then mapped to the human genome (GRCh38 release 84) using Hisat2 (2.1.0) with default settings. Gene expression quantification was calculated using Stringtie (1.3.6). Differential expression analysis was performed by DESeq2 (1.24.0). AR score1 was acquired from the cBioPortal database (www.cbioportal.org) which contains 30 AR responsive genes described previously. AR score2 was calculated using the GSVA method (1.38.2) in R (3.6.1) based on 10 AR responsive genes adopted from a previous publication. The PCa patient RNA-Seq data was accessed in dbGaP with accession phs000915.v2.p2 and analyzed using the same pipeline. Gene Set Enrichment Analysis was performed using by GSEA (4.0.3) within MSigDBv7.1.

For manuscripts utilizing custom algorithms or software that are central to the research but not yet described in published literature, software must be made available to editors and reviewers. We strongly encourage code deposition in a community repository (e.g. GitHub). See the Nature Portfolio [guidelines for submitting code & software](#) for further information.

Data

Policy information about [availability of data](#)

All manuscripts must include a [data availability statement](#). This statement should provide the following information, where applicable:

- Accession codes, unique identifiers, or web links for publicly available datasets
- A description of any restrictions on data availability
- For clinical datasets or third party data, please ensure that the statement adheres to our [policy](#)

RNA-seq data has been deposit to The National Omics Data Encyclopedia with the accession number: OEP001758.The human prostate cancer transcriptome data

Field-specific reporting

Please select the one below that is the best fit for your research. If you are not sure, read the appropriate sections before making your selection.

- Life sciences Behavioural & social sciences Ecological, evolutionary & environmental sciences

For a reference copy of the document with all sections, see [nature.com/documents/nr-reporting-summary-flat.pdf](https://www.nature.com/documents/nr-reporting-summary-flat.pdf)

Life sciences study design

All studies must disclose on these points even when the disclosure is negative.

- Sample size
- Data exclusions
- Replication
- Randomization
- Blinding

Reporting for specific materials, systems and methods

We require information from authors about some types of materials, experimental systems and methods used in many studies. Here, indicate whether each material, system or method listed is relevant to your study. If you are not sure if a list item applies to your research, read the appropriate section before selecting a response.

Materials & experimental systems

- | n/a | Involved in the study |
|-------------------------------------|---|
| <input type="checkbox"/> | <input checked="" type="checkbox"/> Antibodies |
| <input type="checkbox"/> | <input checked="" type="checkbox"/> Eukaryotic cell lines |
| <input checked="" type="checkbox"/> | <input type="checkbox"/> Palaeontology and archaeology |
| <input type="checkbox"/> | <input checked="" type="checkbox"/> Animals and other organisms |
| <input type="checkbox"/> | <input checked="" type="checkbox"/> Human research participants |
| <input checked="" type="checkbox"/> | <input type="checkbox"/> Clinical data |
| <input checked="" type="checkbox"/> | <input type="checkbox"/> Dual use research of concern |

Methods

- | n/a | Involved in the study |
|-------------------------------------|--|
| <input type="checkbox"/> | <input checked="" type="checkbox"/> ChIP-seq |
| <input type="checkbox"/> | <input checked="" type="checkbox"/> Flow cytometry |
| <input checked="" type="checkbox"/> | <input type="checkbox"/> MRI-based neuroimaging |

Antibodies

Antibodies used

Antibodies Brand Catalog No. Dilution
Phospho-p44/42 MAPK (Erk1/2) (Thr202/Tyr204) Antibody CST 9101 1:1000 for WB; 1:500 for IHC
p44/42 MAPK (Erk1/2) (137F5) Rabbit monoclonal CST 4695 1:1000
MEK1 (MAP2K1) Antibody (N-term) Rabbit monoclonal Abgent AP7904a 1:1000 for WB; 1:500 for IHC
p-MEK1/2(ser217/221)419G CST 9154 1:1000
FGF Receptor 1 (D8E4) XP Rabbit monoclonal CST 9740S 1:1000 for WB; 1:50 for IP; 1:100 for IF
Anti-FGFR1 alpha Mouse monoclonal Abcam ab824 1:1000
FGF Receptor 2 (D4L2V) Rabbit mAb CST 23328 1:1000
Phospho-FGF Receptor 1 (Tyr653/654) (D4X3D) Rabbit monoclonal CST 52928 1:1000 for WB; 1:500 for IHC
GAPDH Rabbit polyclonal Bioworld APO063 1:1000
ACTIN Monoclonal Antibody ABclonal AC026 1:1000
Anti-Prostate Specific Antigen Rabbit polyclonal Abcam Ab53774 1:500
Mouse anti HA abclonal AE008 1:1000
Rabbit anti HA CST 3724S 1:100 for IP
mouse IgG abclonal AC011 1:100
Rabbit anti FLAG abclonal AE004 1:1000
Mouse anti FLAG sigma SLBJ4607V 1:100 for IP
rabbit IgG abclonal AC005 1:100
EGF Receptor (D38B1) XP Rabbit monoclonal CST #4267 1:1000
PCNA (PC10) Mouse monoclonal CST #2586 1:500
Recombinant Anti-Androgen Receptor Rabbit monoclonal Abcam ab133273 1:500 for IHC
1:1000 for WB
Annexin V Apoptosis Detection Kit APC eBioscience™ 88-8007-72 1:100

E-Cadherin (24E10) Rabbit monoclonal CST #3195 1:500
 Vimentin (D21H3) XP Rabbit monoclonal CST #5741 1:500
 Anti-BMPRII antibody CST 6979S 1:1000
 Goat anti-Rabbit HRP CST #7074 1:5000
 Goat anti-Mouse HRP CST #7076 1:5000
 Alexa Fluor™ 488 donkey anti-mouse IgG(H+L) Life Technologies A21202 1:800
 Alexa Fluor 594 donkey anti-rabbit IgG(H+L) Life Technologies A21207 1:800
 Caspase 3/P17/P19 Polyclonal Antibody proteintech 19677 1:1000
 Cleaved Caspase-3 (Asp175) Antibody CST 9661 1:1000
 Phospho-FGFR2 (Ser782) Polyclonal Antibody Invitrogen PA5-64796 1:1000
 PLCγ1 (D9H10) XP® Rabbit mAb CST 5690 1:1000
 Phospho-PLCγ1 (Tyr783) (D6M9S) Rabbit mAb CST 14008 1:1000
 Phospho-Akt (Ser473) (D9E) XP® Rabbit mAb CST 4060 1:1000
 Akt (pan) (C67E7) Rabbit mAb CST 4691 1:1000
 Androgen Receptor (D6F11) XP Rabbit mAb CST 5153 1:100 for ChIP

Validation

The anti-human Gremlin1 antibody (MabSpace Biosciences) was utilized to perform immunoblotting, IF, IHC, and IP assays. The specificity assessment of the anti-human Gremlin1 antibody in immunoblotting, IF, IHC and IP assays was validated using GREM1 overexpressing, and GREM1 knockout LNCaP cells and their respective controls (Extended Data 10). Other commercial antibodies used in this study were utilized according to manufacturer's website.

Eukaryotic cell lines

Policy information about [cell lines](#)

Cell line source(s)

The PC3, LNCaP and VCaP cell lines were obtained from the American Type Culture Collection. The LAPC4 cell line was kindly shared by Prof. Charles Sawyers at Memorial Sloan Kettering Cancer Center. LLNCaP-R was derived from LNCaP cells implanted in castrated male nude mice. VCaP-R was generated from VCaP cells treated with charcoal/dextran-stripped serum for three weeks. Patient-derived organoid lines BM1, BM61, ST88 and ST60 were kindly provided by Prof. Dong Gao at Chinese Academy of Sciences, Shanghai. Patient-derived xenograft MDA PCa 118b was generously shared by Prof. Nora M. Navone at the University of Texas MD Anderson Cancer Center.

Authentication

The PC3, LNCaP, VCaP and LAPC4 cell lines were validated at Shanghai Biowing Applied Biotechnology by short Tandem Repeat (STR) profiling.

Mycoplasma contamination

The Cell lines were tested for mycoplasma contamination using TransDetect® PCR Mycoplasma Detection Kit (TRANS, China) and all lines were negative in the test.

Commonly misidentified lines
(See [ICLAC](#) register)

No commonly misidentified cell lines were used in the study.

Animals and other organisms

Policy information about [studies involving animals](#); [ARRIVE guidelines](#) recommended for reporting animal research

Laboratory animals

Athymic nu/nu male mice (6-week-old) and SCID mice were purchased from Shanghai Slac laboratory animal company. Pbsn-Cre4, Ptenfl/fl, and Trp53fl/fl were obtained from the Jackson Laboratory. Hi-Myc mice were provided by the NCI mouse repository. All animals were raised under specific pathogen-free conditions with 12/12 h light/dark cycle and controlled temperature and humidity, at the animal facility of Renji hospital. All the animals were fed with chow diet (the catalogue number is P1101F-25 from Shanghai Slac laboratory animal company). Mice were sacrificed before tumor volume reached 2000 mm³.

Wild animals

The study did not involve wild animals.

Field-collected samples

No field collected samples were used in the study.

Ethics oversight

The Ren Ji Hospital Laboratory Animal Use and Care Committee.

Note that full information on the approval of the study protocol must also be provided in the manuscript.

Human research participants

Policy information about [studies involving human research participants](#)

Population characteristics

Human prostate tissues from hormone sensitive (HSPC) and castration resistant prostate cancer (CRPC) samples were collected from biopsies or prostatectomy surgery. Prostatic fluid and the tumor samples were collected from the patients from 50 to 85 years old diagnosed with prostate cancer at the Urology department of Ren Ji Hospital.

Recruitment

All patients were Patients diagnosed with prostate cancer from 50 to 85 years old were recruited. The diagnosis of HSPC or CRPC was based on both histological examination and the expression of AR related markers by certified pathologists in Department of Pathology, Ren Ji Hospital. All specimens were obtained with patient informed consent.

Ethics oversight

The Ethic Committee at Ren Ji Hospital, School of Medicine, Shanghai Jiao Tong University.

ChIP-seq

Data deposition

- Confirm that both raw and final processed data have been deposited in a public database such as [GEO](#).
- Confirm that you have deposited or provided access to graph files (e.g. BED files) for the called peaks.

Data access links

May remain private before publication.

ChIP-seq data have been deposited at The National Omics Data Encyclopedia with the accession number: OEP001758.

Files in database submission

```
LNCAP_G_0_AR_rep1_1.fq.gz
LNCAP_G_0_AR_rep1_2.fq.gz
LNCAP_G_0_AR_rep2_1.fq.gz
LNCAP_G_0_AR_rep2_2.fq.gz
LNCAP_G_0_INPUT_1.fq.gz
LNCAP_G_0_INPUT_2.fq.gz
LNCAP_G_10_AR_rep1_1.fq.gz
LNCAP_G_10_AR_rep1_2.fq.gz
LNCAP_G_10_AR_rep2_1.fq.gz
LNCAP_G_10_AR_rep2_2.fq.gz
LNCAP_G_10_INPUT_1.fq.gz
LNCAP_G_10_INPUT_2.fq.gz
LNCAP_V_0_AR_rep1_1.fq.gz
LNCAP_V_0_AR_rep1_2.fq.gz
LNCAP_V_0_AR_rep2_1.fq.gz
LNCAP_V_0_AR_rep2_2.fq.gz
LNCAP_V_0_INPUT_1.fq.gz
LNCAP_V_0_INPUT_2.fq.gz
LNCAP_V_10_AR_rep1_1.fq.gz
LNCAP_V_10_AR_rep1_2.fq.gz
LNCAP_V_10_AR_rep2_1.fq.gz
LNCAP_V_10_AR_rep2_2.fq.gz
LNCAP_V_10_INPUT_1.fq.gz
LNCAP_V_10_INPUT_2.fq.gz
```

Genome browser session

(e.g. [UCSC](#))

<http://genome.ucsc.edu/cgi-bin/hgTracks?db=hg38>

Methodology

Replicates

We have generated a minimum of two independent biological replicates from ChIP-seq experiments, with exception of input samples, for which only one biological replicate was generated for preliminary assessment

Sequencing depth

ChIP-seq samples were sequenced in Illumina Novaseq in a pair-end 150 bp. All samples showed >90% reads with high quality mapping to hg38.

Antibodies

Androgen Receptor (D6F11) XP® Rabbit mAb - ChIP Grade Cell Signaling Cat# 5153

Peak calling parameters

Peak calling was not performed in this manuscript

Data quality

```
# clean reads and quality control
trim_galore -j 6 -q 25 --phred33 --length 36 --stringency 3 -e 0.1 --paired $PWD/0.raw_data/{_}1.fq.gz $PWD/0.raw_data/{_}2.fq.gz --
fastqc --gzip -o $PWD/1.clean_data/

# read mapping
bowtie2 -p 32 -x $bowtie2_index_human_GRCh38 -1 $PWD/1.clean_data/{_}1_val_1.fq.gz -2 $PWD/1.clean_data/{_}2_val_2.fq.gz -S
$PWD/3.bowtie2/{_}.sam
```

Software

cutadapt 2.6, fastqc 0.11.9, bowtie2 2.3.5, samtools 1.9, picard 2.25.5, deeptools, 3.3.1

Plots

Confirm that:

- The axis labels state the marker and fluorochrome used (e.g. CD4-FITC).
- The axis scales are clearly visible. Include numbers along axes only for bottom left plot of group (a 'group' is an analysis of identical markers).
- All plots are contour plots with outliers or pseudocolor plots.
- A numerical value for number of cells or percentage (with statistics) is provided.

Methodology

Sample preparation

PCa cells were digested and washed two times in a large volume of washing buffer. Single cell suspensions were incubated with Annexin V-APC (eBioscience) and DAPI (Sigma) for 5-15mins at RT. Cells were washed before FACS acquisition.

Instrument

BD fortessa flow cytometer

Software

FolwJo software is used for FACS data analyses.

Cell population abundance

We compared the apoptotic stage cells with the PCa cells with different treatment. The post-sort fractions are shown in the Extended data 10.e. Apoptotic, APC+DAPI-: 2.38%; Dead, APC+DAPI+:3.95%

Gating strategy

Cells were gated by FSC/SSC. Cell without any staining were used as the negative control. Then, the early apoptotic stage cells were identified based on APC+/DAPI-.

- Tick this box to confirm that a figure exemplifying the gating strategy is provided in the Supplementary Information.